NASA Technical Memorandum 74095

Pressure and Heat-Transfer Distributions in a Simulated Wing-Elevon Cove With Variable Leakage at a Free-Stream Mach Number of 6.9

William D. Deveikis and Whitney Bartlett

DECEMBER 1978

NASA Technical Memorandum 74095

Pressure and Heat-Transfer Distributions in a Simulated Wing-Elevon Cove With Variable Leakage at a Free-Stream Mach Number of 6.9

William D. Deveikis and Whitney Bartlett
Langley Research Center
Hampton, Virginia

National Aeronautics
and Space Administration

**Scientific and Technical
Information Office**

1978

SUMMARY

A full-scale model that represented a section of the cove region between the wing and elevon on the windward surface of the space shuttle orbiter was tested in the Langley 8-foot high-temperature structures tunnel to determine effects of hot boundary-layer ingestion into the cove as a function of seal leak area. Pressure and heating-rate distributions were obtained on the wing and elevon surfaces and on the cove walls for attached and separated turbulent boundary layers upstream of the unswept cove entrance. Cove leakage was controlled by means of a slotted seal located near the elevon hinge line. Length and height of the slot were varied to provide leak areas between 0 and 100 percent of cove entrance area and to simulate both local and general seal failures. For tests with attached flow, wing angle of attack and elevon deflection were varied up to 12° and 15°, respectively. For tests with separated flow, a ramp was attached to the elevon near the cove entrance to provide a deflection of 55° and thus force boundary-layer separation from the wing surface. Average free-stream Mach number was 6.9, average free-stream unit Reynolds numbers were 1.31×10^6 and 4.40×10^6 per meter (0.40×10^6 and 1.34×10^6 per foot), and average total temperature was 1888 K (3400° R).

As the simulated seal failure was increased from a small localized leak to a major leak, the cove environment varied as a function of leak area independent of the shape of the leak. Cove pressures were uniform between the entrance and the seal and decreased with leakage. Cove heating rates decreased with distance from the entrance but increased with leakage. With attached flow on the wing at the cove entrance and for an angle of attack of 12° and elevon deflection of 10°, cove pressures varied from 57 percent of wing pressure at zero leakage to 20 percent at maximum leakage. At zero leakage, cove cold-wall heating rates decreased from 2 percent of wing heating rate near the entrance to 0.07 percent at the seal. At maximum leakage, the heating rates varied between 23 percent and 6 percent of wing heating rate. With separated flow at zero and maximum leakage, cove pressures and heating rates approached, matched, or exceeded wing surface values. Cove pressures exceeded attached-flow cove pressures by 1 order of magnitude, and cove heating rates exceeded attached-flow cove heating rates by more than 2 orders of magnitude.

INTRODUCTION

On shuttle-type winged reentry vehicles and hypersonic cruise aircraft, differential pressure across the wing promotes ingestion of boundary-layer gas into the spanwise clearance, or cove, on the lower surface between the wing and its control surfaces as illustrated in figure 1. This figure shows the current space shuttle orbiter at high angle of attack during reentry and a simplified illustration of the structure at the juncture between the wing and elevon. In cross section, the cove is a curved channel bounded by a concave cylindrical wall on the wing and a mating concentric wall formed by the leading edge of the elevon. On the upper surface of the wing, insulated titanium hinged panels

accommodate contour changes during elevon rotation but also provide outlets through which ingested flow from the lower surface can pass. Although both the upper and lower surfaces are thermally protected with reusable surface insulation (RSI), the interior aluminum structure is not. According to reference 1, predicted temperatures on the lower surface of the orbiter wing are as high as 1280 K (2300° R) near the outboard elevon during reentry (shaded region on orbiter sketch in fig. 1). Obviously, thermally unprotected load-bearing structures exposed to ingested boundary-layer gas at that level of heating would be endangered. Therefore, the use of seals, such as the spring-loaded polyimide wiper shown at the hinge axis (fig. 1), to retard ingestion and thus isolate the interior structure without impeding control-surface articulation has become an important design consideration for such vehicles. In designing seals for this purpose, the possibility of seal failure cannot be overlooked; thus, it is also important to know how much leakage can be tolerated and whether even a small localized leak will threaten the interior structure.

At present, there are no reliable analytical methods available for accurately predicting cove pressures and heating rates, and most of the available experimental data were obtained using small wedge-flap models, as reported, for example, in references 2 and 3. Although a full-scale model that was geometrically and structurally similar to the shuttle orbiter cove was used in the investigation of reference 4, it was tested in the wall of a narrow-duct (5.08-cm-high (2.00-in.)) arc tunnel at zero elevon deflection. Consequently, the Langley Research Center initiated a wind-tunnel test program using the hypersonic aerothermal environment of the Langley 8-foot high-temperature structures tunnel and a heavily instrumented, sting-mounted model with a rotatable control surface. The full-scale model represented a section of the windward surface of the space shuttle orbiter at the wing-elevon juncture and permitted detailed observations that were not possible with a small-scale model. Cove leakage was controlled by means of a slotted seal near the elevon hinge line. Length and height of the slot were varied to provide nominal leak areas between 0 and 100 percent of cove entrance area and to simulate both localized and general seal failures up to 105 cm (41.25 in.) in length.

Pressures and temperatures were obtained on the wing and elevon external surfaces, on both cove walls, and in the cove stream for attached and separated turbulent boundary layers upstream of the cove entrance, which was unswept with respect to the tunnel flow. For tests with attached flow, wing angle of attack and elevon deflection angle were varied up to 12° and 15°, respectively. For tests with separated flow, a ramp was attached to the elevon surface near the cove entrance to provide a deflection of 55° and thus force boundary-layer separation from the wing surface. Average free-stream Mach number was 6.9, average free-stream unit Reynolds numbers were 1.31×10^6 and 4.40×10^6 per meter (0.40×10^6 and 1.34×10^6 per foot), and average total temperature was 1888 K (3400° R). Preliminary data are presented herein. Centerline data from all tests are tabulated, but only results from selected tests are plotted and discussed to show trends and to illustrate major conclusions. For these tests, the free-stream Reynolds number based on the distance to the cove entrance was nominally 5.44×10^6, and calculated boundary-layer thickness at the cove entrance was 2.16 cm (0.85 in.).

Use of trade names or names of manufacturers in this report does not constitute an official endorsement of such products or manufacturers, either expressed or implied, by the National Aeronautics and Space Administration.

SYMBOLS

Values are given both in SI Units and in U.S. Customary Units. The measurements and calculations were made in U.S. Customary Units.

A	area, cm^2 (in^2)
h	height of seal leak, cm (in.)
l	length of seal leak, cm (in.)
M	Mach number
p	pressure, Pa (psia)
$\bar{p}$	average cove pressure, Pa (psia)
Δp	differential pressure, Pa (psi)
q	dynamic pressure, Pa (psi)
$\dot{q}$	heating rate, W/m^2 (Btu/ft^2-sec)
r	cove radius (fig. 4), cm (in.)
R	Reynolds number
s	surface distance referenced from a location on wing (table I)
s'	surface distance referenced from elevon leading edge (table I)
T	temperature, K (^oR)
y	height of slotted cove seal (fig. 5), cm (in.)
α	wing angle of attack, deg
δ	elevon deflection angle, deg

Subscripts:

att	attached flow
c	thermocouple location (fig. 6)
e	cove entrance

g	gas
l	leak
ref	reference location on wing (table I)
t	total condition in combustor
1,2,3,...,31	orifice and wall thermocouple locations (table I and fig. 6)
∞	free stream

MODEL, FACILITY, AND TESTS

Model

Configuration.- The model, shown installed in a sting-mounted flat test bed in figure 2, consisted of a fixed wing-cove housing, a rotatable elevon, and aerodynamic fences at the sidewalls to channel the upstream surface flow across the cove entrance. The wing surface was flush with the test-bed surface. The cove entrance, which was located 124 cm (49 in.) downstream from the sharp leading edge, was unswept with respect to the longitudinal axis of the test bed and, hence, to the tunnel flow. Turbulent flow across the cove entrance was assured with the aid of a boundary-layer trip of 0.24-cm-diameter (0.094-in.) spheres spaced across the width of the test bed and located near the leading edge. Flow conditions along the wing surface were varied by pitching the test bed. The test bed was approximately 300 cm (10 ft) long, 141 cm (4.6 ft) wide, and 30 cm (1 ft) deep.

As indicated by the illustration in figure 3, the wing-cove housing was constructed of aluminum and the elevon of mild steel. The wing and elevon surfaces were covered with 1.27-cm-thick (0.50-in.) Glasrock[1] tiles for thermal protection from the aerothermal environment produced in the wind tunnel. The stainless-steel blocks and centerline strip shown in the Glasrock surfaces contained pressure orifices and thermocouples. Cove span was 105 cm (41.25 in.), and elevon chord from the hinge axis was 61 cm (24 in.). The elevon sidewalls were hinged to the aerodynamic fences, and the sidewalls of both the wing-cove housing and elevon were sealed against the fences. Thus, flow along the wing surface could ingress only at the cove entrance, and flow along the elevon surface could not leak into the cavity under the elevon to influence internal pressure distribution. A cross section of the wing, cove, and elevon arrangement is shown in figure 4. The method of sealing the cove was based on an early shuttle orbiter design in which the seal was flex-spring supported from the elevon and wiped against a cylindrical rub surface as shown in figure 4(a). The rub surface was a machined stainless-steel plate of radius 8.59 cm (3.38 in.) and represented the rub tube shown at the orbiter elevon hinge axis in figure 1. The seal used in the model was a 0.95-cm-thick (0.375-in.) machined cast-iron bar. The cove-elevon configuration approximated that of the

---

[1]Glasrock: Trade name of Glasrock Products, Inc.

space shuttle orbiter in that the cove wall radius on the wing-cove housing was 16.5 cm (6.50 in.) and the radius of the elevon leading edge was 15.24 cm (6.00 in.) as shown in figures 4(b) and 4(c). A seal leak was simulated by a machined slot in the bar, as illustrated in figure 5. Both the length and height of the slot were varied to simulate small localized seal failures as well as major seal failures over a range of 13 leak areas from 0 to approximately 100 percent of cove entrance area. As indicated, slot lengths were 2.54 cm (1.00 in.), 30.48 cm (12.00 in.), and 105 cm (41.25 in.) (full span). For each length, the slot height was varied to a maximum of nominally 1.27 cm (0.50 in.). To change the height of a full-span slot, the rub plate was displaced by removing shims under it. For full-span slots, the rub surface and seal were distorted by end loads from the fences with the result that the height of the slot varied along the span. This discrepancy was not accounted for in reference 5, but full-span leak areas herein have been corrected.

During tests in which the elevon was deflected, flow that was admitted into the cove by the leaking seal vented to a region at less than free-stream static pressure at the elevon trailing edge, as illustrated in figure 6. At zero elevon deflection, the internal flow vented through tubes at the base of the test bed that were routed under the test chamber where the static pressure approximated free-stream static pressure.

A detachable flow separator (dashed outline in fig. 6) was used in some tests to force boundary-layer separation ahead of the cove entrance by increasing the flow turning angle. These tests provided a means of determining gross effects on cove environment of the higher pressures associated with a separated boundary layer. The flow separator was employed because the elevon could not be deflected sufficiently without encountering tunnel flow breakdown. The separator, inclined 45^{o} relative to the elevon, spanned the distance between the fences on the elevon just downstream from the cove entrance and extended to the height of the fences which was approximately 7.62 cm (3 in.).

Instrumentation.- Instrumentation included 63 number 30-gage wire chromel-alumel thermocouples and 58 pressure orifices distributed on the wing, cove, and elevon surfaces and also in the cavity under the elevon. The majority of sensors were placed on or near the centerline, with chordwise distribution as indicated in figure 6, and the remainder were distributed near the side edges as shown in figure 3. On the wing and elevon surfaces, the thermocouples near side edges were located approximately 1.27 cm (0.50 in.) inboard from the side edges, and pressure orifices were located 1.02 cm (0.40 in.) inboard from the thermocouples. Also included, as shown in figure 6, were unshielded beaded thermocouples located in the space between the cove walls near the cove entrance (location a), ahead of the seal at three distances normal to the cove wall (location b), and in front of the bulkhead downstream from the seal at five spanwise stations (location c). These thermocouples provided an indication of cove gas temperature response. A pitot pressure probe was located near location b, and there were pressure orifices adjacent to each thermocouple at location c, behind the seal at location 14, under the elevon at location 31, and at the base of the elevon at location 30.

For wing and elevon wall temperature measurements, individual thermocouple wires were spot-welded to the back face of thin-wall sections that were machined

into the stainless-steel blocks and centerline strip shown in figure 3. The thickness of the thin-wall sections varied between approximately 0.074 cm (0.030 in.) and 0.15 cm (0.060 in.) as listed in table I. (The larger thickness was intended for the flat surface of the elevon where heating rates would be high but was inadvertently machined on the curved leading edge of the elevon.) In the aluminum cove wall, the thermocouple wires were individually spot-welded to the back face of 0.076-cm-thick (0.030-in.) stainless-steel discs that were bonded with silicone rubber (RTV 560) to counterbored holes in the surface. The wall thermocouples provided data from which cold-wall heating rates could be evaluated. Pressure measurements were obtained with the aid of strain-gage transducers that were connected to short lengths of 0.15-cm-inside-diameter (0.060-in.) stainless-steel orifice tubing. Surface distances to centerline surface instrumentation used in data plots are listed in table I.

Facility

The tests were conducted in the Langley 8-foot high-temperature structures tunnel. This facility, schematically illustrated in figure 7, is a hypersonic blowdown wind tunnel that operates at a nominal Mach number of 7, at total pressures between 4.1 and 24.1 MPa (600 and 3500 psia), and at nominal total temperatures between 1389 and 2000 K (2500° and 3600° R) for free-stream unit Reynolds numbers between 10^6 and 10^7 per meter (0.3×10^6 and 3.0×10^6 per foot). The test medium is the combustion products of methane and air which are produced in a high-pressure combustor, expanded through an axisymmetric contoured nozzle 2.4 m (8 ft) in diameter at its exit, and diffused and pumped from the test section to the atmosphere by means of a single-stage annular air ejector. In the test section, the stream is a free jet 4.3 m (14 ft) in length with a usable test core approximately 1.2 m (4 ft) in diameter. During tunnel startup, models are stored in the pod below the test stream until the desired hypersonic flow conditions are established; the model is then inserted into the stream by means of a hydraulically actuated elevator and withdrawn prior to termination of tunnel flow. In the present tests, the test bed reached the stream centerline 1 sec after entering the stream. More detailed information on this facility is reported in reference 6.

Tests

The present investigation comprised 37 tests with attached flow on the wing at the cove entrance and 4 tests with separated flow. Test conditions are listed in table II. For tests with attached flow, all 13 leak configurations indicated in figure 5 were investigated, but for tests with separated flow, only the configurations for zero and maximum leakage ($h = 0$ and 1.27 cm (0.50 in.) by $\ell = 105$ cm (41.25 in.)) were investigated. Average free-stream Mach number for all tests was 6.9, and average total temperature was 1888 K (3400° R). Average free-stream dynamic pressures were 15 and 61 kPa (2.17 and 8.85 psi). Corresponding average free-stream unit Reynolds numbers were 1.31×10^6 and 4.40×10^6 per meter (0.40×10^6 and 1.34×10^6 per foot). However, two Reynolds numbers between these limits were included in tests at maximum leakage for attached flow (tests 36 and 37, table II). Effects on cove environment at maximum leakage can, therefore, be observed at four

Reynolds numbers. Most tests for attached flow were conducted with the wing surface pitched 12° and elevon deflected 10°, but for some tests at 50- and 100-percent leak areas, the elevon was also deflected 5°. For some tests at zero leakage, the wing surface was pitched 10° for elevon deflections of 0°, 10°, and 15°. For the tests with separated flow, the elevon was deflected 10° which inclined the flow separator at 55° relative to the wing surface. This inclination was not intended to simulate a flight condition but only to ensure that flow separation would occur. For zero leakage tests with separated flow, wing pitch angles were 0° and 12° at low Reynolds number. For maximum leakage tests with separated flow, wing pitch angle was 0° at the low Reynolds number and was swept from 5° to 12° at the high Reynolds number. Aerodynamic exposures were less than 20 sec.

Data Acquisition and Reduction

Outputs from pressure transducers and thermocouples were recorded on magnetic tape at a rate of 20 samples per second. All data were reduced to engineering quantities at the Langley central digital data recording facility. Computed quantities reported herein are based on the thermal, transport, and flow properties of the combustion-products test medium as reported in reference 7. Free-stream conditions in the test section were determined from reference measurements in the combustor (fig. 7) by using results from tunnel-stream survey tests as presented, for example, in reference 8. Wing and elevon surface Mach numbers were determined from oblique-shock relations based on a ratio of specific heats for methane-air combustion products (average ratio from all tests was 1.38). Transient heat-conduction calculations indicated that heat loss by conduction was negligible within the first second of aerodynamic exposure. Therefore, heat-transfer data were evaluated at the end of the first second in the stream.

RESULTS AND DISCUSSION

Summary of Test Results

Pressures and cold-wall heating rates on the wing, elevon, and cove walls, normalized with respect to wing surface conditions, are presented for all tests in tables III and IV. (Data presented herein for full-span leaks are based on the corrected measurements of full-span slot height given in fig. 5.) These results indicated little effect of elevon deflection on wing pressures, wing heating rates, and cove pressures, but cove heating rates tended to increase with elevon deflection. As free-stream Reynolds number increased, normalized cove pressures and heating rates also increased. However, inasmuch as the trends in the distribution of the data within the cove did not change significantly with free-stream Reynolds number, attached-flow data are discussed in the next section only for the high Reynolds number and for $\alpha = 12^\circ$ and $\delta = 10^\circ$. The separated-flow data are discussed in a subsequent section.

Attached Flow

Exterior surface pressures and heating rates.- Typical normalized pressure and heating-rate distributions on the wing and on the flat surface of the elevon are pictorially represented in figure 8. As indicated, wing centerline pressures and heating rates approaching the cove entrance were relatively uniform, whereas elevon centerline pressures and heating rates increased toward the trailing edge to 3.6 times the wing pressure and 2.6 times the wing heating rate. Values near the side edges where the fences extended above the wing and elevon surfaces were higher than at the centerline as a result of a corner effect. Values at the elevon trailing-edge corners, where the deflected elevon surface extended above the fences, were lower than at the centerline as a result of flow spillage. Nominal surface flow conditions were as follows: centerline wing and elevon pressures were 10.3 and 33.8 kPa (1.5 and 4.9 psia), respectively; wing and elevon centerline cold-wall heating rates were 193 and 567 kW/m^2 (17 and 50 Btu/ft^2-sec), respectively; and wing and elevon surface Mach numbers were 4.8 and 3.8, respectively. The wing values were consistent with values reported in reference 8 for a flat plate tested in the same test bed and in the same facility as in the present investigation; hence, wing values were not affected by the deflected elevon. Consequently, it was concluded that the flow was attached to the wing at the cove entrance.

Centerline pressure distributions.- Centerline pressure distributions on the wing and elevon, in the cove, and in the cavity behind the seal are presented normalized with respect to wing pressure in figure 9. The data are shown for the sealed cove and for maximum leakage to illustrate the extent of the change in cove pressure that occurred over the total range of leak size investigated. A comparison of the wing and elevon aerodynamic surface data with calculated values from oblique-shock theory (dashed curves) indicates that wing pressures were predicted to within 3 percent and that elevon pressures exceeded the oblique-shock value by about 20 percent. These results are consistent with the agreement obtained from previous investigations in the same facility (refs. 8 and 9).

Pressures in the cove were essentially equal on opposite walls and were uniform between the cove entrance and the rub surface; all pressures behind the seal (square symbols in fig. 9) increased with leak area but remained less than cove pressures and also less than free-stream static pressure. As leak area was increased from $A_l/A_e = 0$ to 1.04, pressures in the cove decreased from 57 percent to approximately 20 percent of wing pressure, and differential pressure across the seal decreased from 4.8 kPa to 0.3 kPa (0.7 to 0.4 psi). The pressure distributions in figure 9 also indicate that flow reattachment on the elevon moved upstream as leak area increased (illustrated on the sketch of the elevon in fig. 9). This effect was deduced from the change in location of the local rise in elevon surface pressure identified by the arrows on the elevon pressure distributions. Sketches of simplified flow patterns based on these data are shown in figure 10. These patterns indicate that, both for sealed (fig. 10(a)) and unsealed (fig. 10(b)) coves, the flow apparently expanded around part of the rounded trailing edge of the wing before it bridged the gap across the cove entrance and reattached to the elevon. This effect probably accounts, in part, for the depressed pressures obtained in the sealed cove. When the cove was unsealed, flow was introduced through the cove

by the low-pressure region behind the seal which further reduced cove pressures, increased flow expansion at the cove entrance, and moved flow reattachment upstream as in figure 10(b).

Normalized centerline pressure distributions obtained on both cove walls are presented in figure 11 for all of the full-span leaks to indicate the changes that occurred as leak area increased from zero to maximum. Elevon data are superimposed on wing-cove data. For A_l/A_e up to 0.16, the distributions appear relatively uniform throughout the cove. In this range of leak area, downstream-to-upstream pressure ratios across the seal, as listed in table III, indicated the presence of sonic conditions at the leak ($p_{14}/p_{10} < 0.528$ in air and 0.537 in methane-air combustion products; cove pressures in this range of leak area were essentially equivalent to the pressure given by a total pressure probe at location b, fig. 6). For $A_l/A_e > 0.16$, perturbations occurred such as a local overexpansion on the elevon curved surface near the cove entrance and a local rise in pressure at the apex of the cove path (orifice 9 at $s/r = 2.6$) for maximum A_l/A_e. The former was probably associated with the flow reattachment process in which part of the flow is turned into the cove following impingement, whereas the latter probably resulted from flow deceleration in the turn at the apex.

Centerline heating-rate distributions.- Centerline cold-wall heating rates that were obtained on the wing and elevon and in the cove are presented normalized with respect to wing heating rates in figure 12. The data are shown for the sealed cove and for maximum leakage to illustrate the extent of the change in cove heating rates that occurred over the total range of leak size investigated. Also shown are calculated values of the wing and elevon aerodynamic surface heating rates obtained from Eckert's reference enthalpy method using pressures calculated from oblique-shock theory (dashed curve). Although difficult to see from the scale used in plotting these data, the calculated heating rates overpredicted wing and elevon test values near the cove entrance by 30 percent but matched the test value at the elevon trailing edge. The agreement at the trailing edge is considered fortuitous and resulted from use of the underpredicted calculated elevon pressure. The trend of the elevon heating-rate data was better predicted when measured elevon pressures were used (dot-dash curve), but the calculated values exceeded test values by about 25 percent. In making these calculations, the virtual origin for the boundary layer was placed at the leading edge of the test bed. Calculations of elevon heating rates based on a location of the virtual origin at flow impingement on the elevon were unreasonably high (by factors greater than 6) with respect to test data.

In contrast to the cove pressure distributions, which were uniform and decreased as leak area increased, cove heating rates decreased with distance from the cove entrance as shown, but the level of heating within the cove increased as leak area increased. These cove heating trends and the corresponding trends of cove pressures were consistent with the results reported in reference 3 and hypothesized in reference 4. As A_l/A_e increased from 0 to 1.04, the cold-wall heating rate increased near the cove entrance ($s/r = 1.4$) from 2 to 23 percent of wing heating rate and near the seal ($s/r = 3.3$) from 0.07 to 6 percent of wing heating rate. In terms of actual values, these changes amounted to an increase near the cove entrance from

about 5 to 50 kW/m^2 (0.4 to 4 Btu/ft^2-sec) and near the seal from about 0.1 to 11 kW/m^2 (0.01 to 1 Btu/ft^2-sec). Associated with this increase in cove heating was an upstream movement of the location of impingement heating on the elevon from flow reattachment. This effect is indicated as a change in location of the local rise in elevon heating rate identified by the arrows in figure 12. Thus, increased leakage allowed more of the hot boundary-layer flow to turn into the cove and resulted in a steeper flow reattachment angle on the elevon (fig. 10(b)).

Normalized centerline heating-rate distributions obtained on the wing-cove wall are presented in figure 13 for all full-span leaks to indicate the changes that occurred as leak area increased from zero to maximum. For most openings, these data show local increases in heating at the apex of the cove path (thermocouple 9 at $s/r = 2.6$) and on the rub surface just ahead of the seal (thermocouple 12 at $s/r = 3.3$). Although not shown in figure 13, both of these effects were also observed from data for $l = 30$ cm (12 in.), and the latter effect was observed from the data for $l = 2.54$ cm (1 in.). (See table IV.) A local increase in heating at the apex of the cove path was also observed by R. L. Kirlin, D. A. Schmitt, and E. C. Littler of the Martin Marietta Corporation during plasma arc tests in 1974 on a model whose cove configuration was dimensionally similar to that of the present model. However, the cove path for their model was not rounded at the apex but turned a sharp corner instead. From a thermal protection standpoint, the heating rates shown in figure 13 do not appear intolerably severe. Nevertheless, there are indications that convective heating in the cove may be time dependent as will be discussed subsequently.

Temperatures in cove stream.- Responses from the thermocouples in the space between the cove walls are presented in figure 14 for full-span leak area ratios between $A_l/A_e = 0$ and 1.04. The data were normalized with respect to total temperature but were not corrected for thermocouple time lag and heat-sink effects. The temperature data of figure 14(a) were obtained at midstream inside the cove entrance (location a, fig. 6); those shown in figure 14(b) were obtained upstream from the seal rub surface (location b, fig. 6) and at the bulkhead downstream from the seal (location c, fig. 6). The temperatures in figure 14(c) were obtained at three distances from the wall at location b. As indicated, temperatures in the cove stream increased with time and did not reach equilibrium during aerodynamic exposure. These time-dependent responses can be attributed partly to thermocouple time lag and partly to an initial cooling effect on the boundary layer at the cove entrance by the relatively cool wing surface during model entry into the hot tunnel stream. The temperature in the cove stream also increased with increasing leak area but decreased with distance from the cove entrance to the bulkhead (figs. 14(a) and 14(b)). For the sealed cove ($A_l/A_e = 0$), the temperature rise at all locations was very small, but as leak area increased to $A_l/A_e = 1.04$, the temperature near the cove entrance (fig. 14(a)) increased to approximately one-half of total temperature. Upstream from the rub surface (fig. 14(b)), the corresponding temperature rise was to approximately 37 percent of total temperature, and at the bulkhead (fig. 14(b)), it was to approximately 22 percent of total temperature. In figure 14(c), a heat-sink effect of the aluminum cove wall is indicated by a temperature gradient in the cove stream toward the wall for sealed and unsealed coves.

The temperature responses in the cove stream, in conjunction with corresponding responses from cove-wall thermocouples and preliminary results from an ongoing numerical analysis of cove heating, suggest that convective heating in the cove may increase significantly with time. If this postulation is true, then heating rates presented herein are minimum values. Before equilibrium conditions occur on the wing and cove surfaces, some of the stored energy in an element of boundary-layer fluid initially drains to the wing as the element passes over the relatively cool wing surface. As only a small portion of the element is ingested into the cove, its energy continues draining to the cool cove walls, so that very little potential for transferring heat deep inside the cove remains. However, as the temperature of the wing surface and cove walls near the entrance continues rising with aerodynamic exposure, increasing amounts of stored energy may be retained by the ingested fluid element. Consequently, the potential for transferring heat to the cove interior may also increase until steady-state conditions are established. Additional experimentation and analytical work are needed to verify this postulation.

Effect of leak size on cove environment.- As leak area increased, the changing pressures upstream and downstream of the seal resulted in a reduction of differential-pressure loading across the seal from 45 percent of wing pressure for the sealed cove to 2.5 percent of wing pressure at maximum leakage. When plotted as a function of leak area ratio, normalized differential pressures tended to fair as a single curve, as demonstrated in figure 15. For leak areas up to 18 percent of the cove entrance area, sonic conditions occurred at the leak. Within this range of leak area, seal loading progressively decreased by 80 percent.

Likewise, normalized cove heating rates at a given location also correlated with leak area and, as shown in figure 16, increased linearly on a logarithmic plot. In this figure, the heating rates obtained near the cove entrance (location 3, inset), and near the seal (location 10, inset) are shown. The variation for the heating rate near the entrance can be expressed as

$$\frac{\dot{q}}{\dot{q}_{ref}} = 0.23\left(\frac{A_l}{A_e}\right)^{0.415}$$

and for the heating rate near the seal as

$$\frac{\dot{q}}{\dot{q}_{ref}} = 0.07\left(\frac{A_l}{A_e}\right)^{0.697}$$

In the range of leak areas for sonic conditions at the leak (A_l/A_e up to 0.18), heating rates near the seal increased to only 2 percent of wing heating rate. The variations of cove pressures and heating rates with leak area were unaffected by the presence or absence of sonic conditions at the leak. Thus as the simulated seal failure increased from a small localized leak to a major leak, the cove heating environment progressively increased in severity,

strictly as a function of leak area and independent of the shape of the leak. There was no evidence that high levels of heating tended to concentrate at the smaller leaks.

Comparison with other data.- In figure 17, normalized heating rates from the present investigation are compared with data from the previously mentioned tests by Kirlin, Schmitt, and Littler. Present data, indicated by symbols, were obtained at the high Reynolds number for the sealed cove and slotted seals for l = 2.54 cm (1.00 in.) and 30.48 cm (12.00 in.). The data from Kirlin et al. are indicated by a shaded band and were obtained from five tests at a total temperature of 5533 K (9960° R) and a wing surface Mach number of 1.31. In their model, the cove was sealed by means of a flexible curtain that bridged the cove gap near the hinge line; however, the ends of the curtain butted against the sidewalls of the model and, hence, were unsealed. As indicated, their data compared most favorably, in terms of average slopes and fair agreement of values, with the present data for the slotted gaps for l = 2.54 cm (1.00 in.). Similar agreement was observed with the present data for the full-span slot for A_l/A_e = 0.032 (fig. 13). In their tests, cove pressure (not shown) averaged 75 percent of wing surface pressure in four tests and 92 percent in the fifth test. These values compare with cove pressures in the present investigation from 57 to 67 percent of wing surface pressure between high and low Reynolds numbers, as given in table III. However, inasmuch as the local Mach number in their tests was substantially less than in the present tests, less flow expansion would have occurred at the cove entrance. Consequently, higher cove pressure ratios would be expected in their tests.

Separated Flow

Use of the flow separator (fig. 6) produced wing surface pressures and cold-wall heating rates that exceeded attached-flow values by factors greater than 4 and 2.5, respectively. The resulting flow pattern across the cove entrance was probably as depicted in figure 18. As indicated, the turbulent boundary layer was forced to turn in the compression direction upstream of the cove entrance and reattach on the flow separator. Consequently, a much more hostile environment ensued than when the boundary layer was attached, as demonstrated by at least tenfold increases in cove pressures and cold-wall heating rates shown in figures 19 and 20. For these figures, the separated-flow data are normalized with respect to attached-flow wing values and are compared with the data at the high Reynolds number for attached flow from figures 9 and 12. In figures 19(a) and 20(a), the sealed-cove data for separated flow were obtained at the low Reynolds number; in figure 20(b), heating rates at maximum leakage for separated flow are shown at $\alpha = 5^\circ$ inasmuch as cold-wall data were not obtained at $\alpha = 12^\circ$. Unlike cove pressures for attached flow, which were always less than wing pressure, cove pressures for separated flow exceeded wing pressure for separated flow at zero leakage (fig. 19(a)) and approached wing pressure for separated flow at maximum leakage (fig. 19(b)). The resulting differential-pressure loading across the seal at zero leakage exceeded the loading for attached flow by a factor of about 12 (compare tests 20 and 38, table III). At maximum leakage, differential pressure across the leak increased relative to attached flow by a factor of about 58 and was sufficient to produce sonic conditions at the leak (compare tests 19 and 41, table III).

Consequently, the bulkhead behind the seal was subjected to a ram pressure approximately equivalent to wing pressure, as indicated in figure 19(b) by the closed square symbol at $s'/r = 1.27$ on the elevon data plot.

As shown in figure 20(a), cold-wall heating rates for the sealed cove increased by 2 orders of magnitude under separated flow and approached attached-flow wing heating rates. At maximum leakage (fig. 20(b)), cold-wall heating rates at $\alpha = 5^{\circ}$ under separated flow were about 1 order of magnitude greater than attached-flow values at $\alpha = 12^{\circ}$ and exceeded attached-flow wing heating rates. Moreover, the temperature obtained in front of the bulkhead behind the seal (location c, fig. 6) increased to $0.5T_t$ after 6 sec as a result of exposure to ram flow. Obviously, the severity of the cove environment generated by the flow separator would be intolerable for unprotected interior structures of control surfaces and would seriously complicate the problem of designing an effective seal.

Although the deflection angle that was applied in forcing flow separation was unrealistic in terms of control-surface deflections that would occur in flight, these results, nevertheless, illustrate the hazardous nature of the environment that can develop in the cove if flow separation is encountered. Additional research is required to obtain a more thorough definition of the cove environment under separated flow at other deflection angles and leak areas.

CONCLUDING REMARKS

A full-scale model that represented a section of the cove region between the wing and elevon on the windward surface of the space shuttle orbiter was tested in a hypersonic wind tunnel (the Langley 8-foot high-temperature structures tunnel) to determine effects of hot boundary-layer ingestion into the cove as a function of seal leak area. Pressure and heating-rate distributions were obtained on the wing and elevon surfaces and on the cove walls for attached and separated turbulent boundary layers upstream of the unswept cove entrance. Cove leakage was controlled by means of a slotted seal located near the elevon hinge line. Length and height of the slot were varied to produce nominal leak areas between 0 and 100 percent of cove entrance area and to simulate both local and general seal failures. For tests with attached flow, wing angle of attack and elevon deflection were varied up to 12° and 15°, respectively. For tests with separated flow, a ramp was attached to the elevon near the cove entrance to provide a deflection of 55° and thus force boundary-layer separation from the wing surface. Average free-stream Mach number was 6.9, average free-stream unit Reynolds numbers were 1.31×10^6 and 4.40×10^6 per meter (0.40×10^6 and 1.34×10^6 per foot), and average total temperature was 1888 K (3400° R). Aerodynamic exposures were less than 20 sec.

The test results for attached flow indicated that the flow expanded around the wing trailing edge at the cove entrance for all leak areas. Cove pressures were uniform and decreased as leakage increased. The results also described a relatively benign cove heating environment that was independent of leak aspect ratio but which progressively increased in severity as the leak area increased from a small localized leak to a major seal failure. There was no evidence

that high levels of heating tended to concentrate at small leaks. For an angle of attack of 12° and elevon deflection of 10°, cove pressures at the high Reynolds number decreased from a value of 57 percent of wing pressure at zero leakage to 20 percent at maximum leakage. Cold-wall heating-rate variation between a location inside the cove entrance and the seal was from about 2 percent to 0.07 percent of wing heating rate at zero leakage and from about 23 percent to 6 percent of wing heating rate at maximum leakage. However, a preliminary analysis of these data suggests that convective heat transfer in the cove increases with time and, therefore, present test results may be minimum values.

When flow was separated over the cove entrance, sealed-cove pressures exceeded the wing pressure for separated flow, differential pressure across the seal increased by a factor of 12, and cold-wall heating rates in the cove increased by 2 orders of magnitude relative to attached-flow values. At maximum leakage, cove pressures approached the wing pressure for separated flow, and differential pressure across the leak subjected a bulkhead behind the seal to ram pressure approximately equivalent to wing pressure. Consequently, the temperature in front of the bulkhead increased to about one-half of free-stream total temperature after 6 sec. Cold-wall heating rates in the cove increased by 1 order of magnitude over attached-flow values and exceeded attached-flow wing heating rates. These conditions are considered too severe for unprotected interior structures of control surfaces and would seriously complicate the problem of designing an effective seal.

Langley Research Center
National Aeronautics and Space Administration
Hampton, VA 23665
November 17, 1978

REFERENCES

1. Strouhal, George; and Tillian, Donald J.: Testing the Shuttle Heat-Protection Armor. Astronaut. & Aeronaut., vol. 14, no. 1, Jan. 1976, pp. 57-65.

2. Hamilton, H. Harris; and Dearing, J. David: Effect of Hinge-Line Bleed on Heat Transfer and Pressure Distribution Over a Wedge-Flap Combination at Mach 10.4. NASA TN D-4686, 1968.

3. Dearing, J. David; and Hamilton, H. Harris: Heat-Transfer and Pressure Distributions Inside the Hinge-Line Gap of a Wedge-Flap Combination at Mach Number 10.4. NASA TN D-4911, 1968.

4. Scott, C. D.; Murray, L. P.; and Milhoan, J. D.: Shuttle Elevon Cove Aerodynamic Heating by Internal Flow. AIAA Paper 77-757, June 1977.

5. Deveikis, William D.; and Bartlett, Whitney: Pressure and Heat-Transfer Distributions in a Simulated Wing-Elevon Cove With Variable Leakage at a Free-Stream Mach Number of 6.9. AIAA Paper 78-39, Jan. 1978.

6. Deveikis, William D.; Bruce, Walter E., Jr.; and Karns, John R.: Techniques for Aerothermal Tests of Large, Flightweight Thermal Protection Panels in a Mach 7 Wind Tunnel. NASA TM X-71983, 1974.

7. Leyhe, E. W.; and Howell, R. R.: Calculation Procedure for Thermodynamic, Transport, and Flow Properties of the Combustion Products of a Hydrocarbon Fuel Mixture Burned in Air With Results for Ethylene-Air and Methane-Air Mixtures. NASA TN D-914, 1962.

8. Deveikis, William D.; and Hunt, L. Roane: Loading and Heating of a Large Flat Plate at Mach 7 in the Langley 8-Foot High-Temperature Structures Tunnel. NASA TN D-7275, 1973.

9. Johnson, Charles B.; Taylor, Allan H.; and Weinstein, Irving: Heat-Transfer and Pressure Measurements on a Simulated Elevon Deflected 30° Near Flight Conditions at Mach 7. NASA TM X-3563, 1977.

TABLE I.- LOCATION OF INSTRUMENTATION ON CENTERLINE

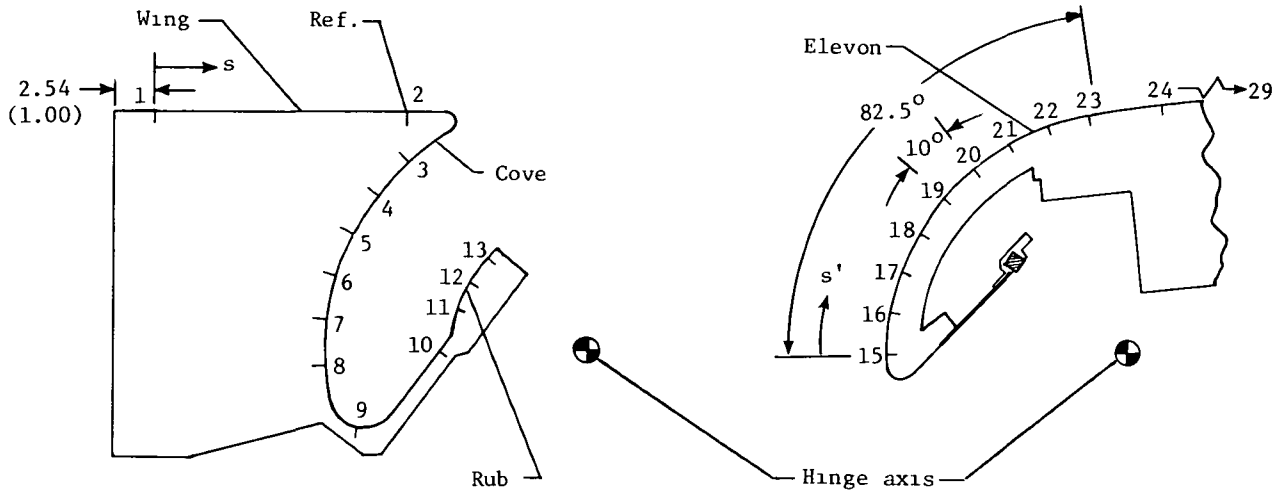

Wing, cove, and rub surfaces						Elevon surface				
Orifice	Thermocouple	s		Wall thickness		Orifice and thermocouple	s'		Wall thickness	
		cm	in.	cm	in.		cm	in.	cm	in.
1	1	0	0	0.079	0.031	15	0	0	0.15	0.058
2 (ref.)	2 (ref.)	16.08	6.33	.076	.030	16	2.62	1.03	.15	.058
3	3	22.91	9.02	.081	.032	17	5.21	2.05	.15	.058
4	4	25.96	10.22	.081	.032	18	7.80	3.07	.15	.058
5	5	29.08	11.45	.081	.032	19	10.49	4.13	.15	.058
6	6	32.05	12.62	.081	.032	20	13.11	5.16	.15	.058
7	7	35.10	13.82	.081	.032	21	15.62	6.15	.15	.058
8	8	38.15	15.02	.081	.032	22	18.29	7.20	.15	.058
9	9	42.67	16.80	.081	.032	23	20.98	8.26	.15	.058
10	10	50.37	19.83	.081	.032	24	25.43	10.01	.097	.038
	11	52.71	20.75	.076	.030	25	29.26	11.52	.097	.038
	12	54.81	21.58	.081	.032	26	36.88	14.52	.102	.040
	13	56.87	22.39	.074	.029	27	44.50	17.52	.102	.040
						28	52.12	20.52	.102	.040
						29	80.06	31.52	.102	.040

TABLE II.- TEST CONDITIONS

Test	h		l		A_l		A_l/A_e	α	δ	T_t	
	cm	in.	cm	in.	cm^2	in^2		deg		K	^oR
Attached flow, high Reynolds number											
1	0	0	105	41.25	0	0	0	9.3	0	1879	3382
2	0	0	105	41.25	0	0	0	9.3	10.0	1893	3407
3	0	0	105	41.25	0	0	0	10.0	14.9	2025	3645
4	0	0	105	41.25	0	0	0	11.8	4.9	1961	3529
5	0	0	105	41.25	0	0	0	12.1	9.8	1902	3423
6	.32	.125	2.54	1.00	.81	.13	.006	12.1	9.8	1885	3393
7	.64	.250	2.54	1.00	1.61	.25	.012	12.1	10.1	1925	3465
8	1.27	.500	2.54	1.00	3.23	.50	.024	12.0	9.7	1949	3509
9	.32	.125	30.48	12.00	9.69	1.50	.073	12.0	9.8	1966	3539
10	.64	.250	30.48	12.00	19.36	3.00	.150	11.9	9.9	1977	3558
11	1.27	.500	30.48	12.00	38.71	6.00	.290	12.1	10.0	1956	3520
12	.02	.008	105	41.25	2.10	.33	.016	11.9	9.5	1958	3525
13	.04	.016	105	41.25	4.31	.66	.032	12.0	9.1	1887	3396
14	.20	.078	105	41.25	21.00	3.22	.160	12.0	9.9	1863	3354
15	.36	.140	105	41.25	37.80	5.78	.280	12.1	9.7	1819	3274
16	.69	.270	105	41.25	72.45	11.14	.540	12.0	4.8	1820	3276
17	.69	.270	105	41.25	72.45	11.14	.540	12.0	9.9	1893	3408
18	1.32	.520	105	41.25	138.60	21.45	1.040	12.0	4.9	2021	3638
19	1.32	.520	105	41.25	138.60	21.45	1.040	12.0	10.0	1943	3497
Attached flow, low Reynolds number											
20	0	0	105	41.25	0	0	0	12.2	10.1	1818	3273
21	.32	.125	2.54	1.00	.81	.13	.006	12.0	9.9	1742	3136
22	.64	.250	2.54	1.00	1.61	.25	.012	12.0	10.3	1662	2992
23	1.27	.500	2.54	1.00	3.23	.50	.024	12.0	9.9	1778	3201
24	.32	.125	30.48	12.00	9.69	1.50	.073	12.0	10.0	1887	3397
25	.64	.250	30.48	12.00	19.34	3.00	.150	12.0	10.0	1777	3199
26	1.27	.500	30.48	12.00	38.71	6.00	.290	11.8	10.1	1813	3263
27	.02	.008	105	41.25	2.10	.33	.016	12.1	10.3	1742	3135
28	.04	.016	105	41.25	4.31	.66	.032	11.9	9.3	1805	3249
29	.20	.078	105	41.25	21.00	3.22	.160	11.9	10.0	1731	3115
30	.36	.140	105	41.25	37.80	5.78	.280	12.1	9.9	1618	2913
31	.69	.270	105	41.25	72.45	11.14	.540	12.0	5.1	1731	3116
32	.69	.270	105	41.25	72.45	11.14	.540	12.0	10.1	1931	3476
33	.69	.270	105	41.25	72.45	11.14	.540	12.0	12.0	1790	3221
34	1.32	.520	105	41.25	138.60	21.45	1.040	12.0	5.0	1922	3460
35	1.32	.520	105	41.25	138.60	21.45	1.040	12.0	10.2	1789	3220
36	1.32	.520	105	41.25	138.60	21.45	1.040	12.0	10.2	1767	3181
37	1.32	.520	105	41.25	138.60	21.45	1.040	12.0	10.2	1647	2964
Separated flow											
38	0	0	105	41.25	0	0	0	12.2	55	1809	3257
39	0	0	105	41.25	0	0	0	0	55	1851	3331
40	1.32	.520	105	41.25	138.60	21.45	1.040	0	55	1739	3131
41	1.32	.520	105	41.25	138.60	21.45	1.040	5 to 12	55	1934	3481

TABLE II.- Concluded

Test	p_t		p_∞		q_∞		M_∞	R_∞		M_{ref}	q_{ref}	
	MPa	psia	kPa	psia	kPa	psi		m^{-1}	ft^{-1}		kPa	psi
Attached flow, high Reynolds number												
1	16.95	2459	1.96	0.285	64.42	9.34	6.80	4.38×10^6	1.34×10^6	5.36	141	20.51
2	16.99	2464	1.96	.284	60.23	8.74	6.81	4.40	1.34	5.24	148	21.53
3	17.33	2514	1.88	.273	61.82	8.97	6.97	4.12	1.26	5.30	154	22.36
4	16.65	2415	1.85	.268	57.45	8.33	6.91	4.07	1.24	4.96	163	23.57
5	16.93	2456	1.94	.282	61.31	8.89	6.83	4.33	1.32	4.90	167	24.16
6	17.46	2532	2.02	.293	64.22	9.32	6.80	4.54	1.38	4.98	166	24.04
7	17.35	2516	1.97	.286	62.24	9.03	6.85	4.40	1.34	4.89	161	23.35
8	-----	----	----	-----	-----	----	----	----------	----------	----	---	-----
9	17.00	2465	1.90	.275	60.73	8.81	6.89	4.21	1.28	4.96	165	23.88
10	17.15	2488	1.90	.275	60.80	8.82	6.91	4.22	1.29	4.94	168	24.30
11	17.15	2487	1.92	.278	58.63	8.50	6.88	4.27	1.30	4.79	165	23.89
12	16.72	2425	1.87	.271	58.63	8.50	6.90	4.17	1.27	4.85	159	23.10
13	17.32	2512	2.01	.291	62.71	9.10	6.80	4.51	1.37	4.95	167	24.20
14	17.70	2567	2.08	.301	66.45	9.64	6.76	4.64	1.41	4.76	168	24.42
15	17.86	2591	2.14	.310	55.72	8.08	6.69	4.81	1.47	4.71	169	24.48
16	17.00	2465	1.99	.288	59.17	8.58	6.75	4.62	1.41	4.82	157	22.74
17	17.77	2578	2.06	.299	62.88	9.12	6.81	4.57	1.39	4.83	168	24.40
18	17.01	2467	1.84	.267	59.73	8.66	6.97	3.99	1.22	5.00	165	23.97
19	17.22	2498	1.93	.280	60.58	8.79	6.86	4.29	1.31	4.89	168	24.42
Attached flow, low Reynolds number												
20	4.45	646	0.48	0.070	15.80	2.29	6.96	1.31×10^6	0.40×10^6	5.05	43	6.18
21	4.19	607	.47	.068	14.49	2.10	6.82	1.14	.35	5.01	39	5.60
22	4.34	630	.50	.072	15.10	2.19	6.67	1.30	.40	4.83	40	5.76
23	-----	----	----	-----	-----	----	----	----------	----------	----	---	-----
24	4.21	611	.44	.064	15.44	2.24	7.08	1.16	.35	5.13	41	5.88
25	4.15	602	.46	.067	15.18	2.20	6.88	1.21	.37	4.98	40	5.75
26	4.13	599	.45	.065	14.87	2.16	6.97	1.11	.34	4.98	40	5.83
27	4.30	623	.48	.070	15.12	2.19	6.82	1.18	.36	5.02	40	5.74
28	4.36	632	.48	.069	15.66	2.27	6.94	1.26	.38	5.06	41	6.01
29	4.31	625	.48	.070	14.74	2.14	6.80	1.29	.39	4.98	41	5.93
30	4.11	596	.47	.068	13.73	1.99	6.58	1.25	.38	4.69	37	5.42
31	4.13	600	.47	.068	14.48	2.10	6.79	1.24	.38	4.89	39	5.70
32	4.16	603	.42	.061	14.44	2.09	7.17	1.11	.34	5.05	41	5.98
33	4.22	612	.47	.068	15.34	2.22	6.90	1.25	.38	4.94	41	5.96
34	4.18	607	.43	.062	15.36	2.23	7.17	1.14	.35	5.12	41	6.01
35	4.15	602	.46	.067	14.76	2.14	6.91	1.21	.37	4.94	41	5.89
36	5.60	812	.62	.090	20.02	2.90	6.95	3.03	.92	5.00	55	7.99
37	6.90	1001	.80	.117	21.43	3.11	6.58	2.06	.63	4.69	64	9.28
Separated flow												
38	4.38	635	.48	0.069	15.44	2.24	6.96	1.30×10^6	0.40×10^6	----	---	-----
39	4.39	636	.47	.068	15.67	2.27	7.02	1.24	.38	----	---	-----
40	4.47	649	.50	.073	15.77	2.29	6.82	1.46	.45	----	---	-----
41	17.01	2467	1.93	.280	60.54	8.78	6.85	4.30	1.31	----	---	-----

TABLE III.- NORMALIZED PRESSURES

Test	A_l/A_e	p_{ref}		$p_{14}/\bar{p}$	Wing	Cove								Bulkhead	Cavity	
		kPa	psia		p_1/p_{ref}	p_3/p_{ref}	p_4/p_{ref}	p_5/p_{ref}	p_6/p_{ref}	p_7/p_{ref}	p_8/p_{ref}	p_9/p_{ref}	p_{10}/p_{ref}	p_c/p_{ref}	p_{14}/p_{ref}	p_{31}/p_{ref}
Attached flow, high Reynolds number																
1	0	7.120	1.033	0.586	1.065	0.580	0.576	0.578	0.580	0.581	0.572	0.582	0.586	0.344	0.342	0.342
2	0	7.810	1.133	.192	1.015	.548	.548	.551	.553	.552	.545	.552	.551	.107	.106	.110
3	0	7.950	1.153	.169	1.016	.550	.547	.550	.549	.548	.538	.545	.542	.092	.092	.091
4	0	9.550	1.385	.279	1.028	.560	.557	.561	.562	.563	.554	.563	.562	.158	.157	.156
5	0	10.040	1.456	.189	1.018	.558	.561	.564	.565	.564	.556	.563	.559	.107	.106	.109
6	.006	9.640	1.398	.229	1.101	.561	.558	.562	.565	.565	.556	.564	.563	.128	.128	.128
7	.012	9.710	1.408	.213	1.076	.546	.543	.546	.548	.549	.540	.548	.549	.114	.116	.113
8	.024	9.630	1.379	.264	1.042	.508	.506	.508	.510	.511	.502	.511	.512	.128	.134	.129
9	.073	9.670	1.403	.323	1.039	.433	.429	.434	.438	.437	.428	.435	.435	.129	.141	.137
10	.150	9.920	1.438	.485	1.052	.303	.305	.306	.307	.307	.303	.308	.304	.132	.148	.136
11	.290	10.390	1.507	.675	1.030	.239	.242	.243	.243	.243	.240	.243	.233	.186	.162	.147
12	.016	9.780	1.418	.231	1.036	.528	.525	.528	.529	.528	.518	.522	.518	.127	.125	.122
13	.032	9.830	1.426	.291	1.050	.493	.492	.496	.498	.497	.489	.495	.494	.145	.144	.147
14	.160	10.740	1.558	.517	1.025	.256	.263	.264	.263	.264	.263	.266	.261	.135	.135	.137
15	.280	10.980	1.592	.643	1.017	.230	.235	.236	.236	.237	.235	.238	.234	.148	.151	.149
16	.540	9.760	1.415	.956	1.022	.225	.229	.230	.228	.232	.232	.235	.230	.225	.218	.222
17	.540	10.750	1.559	.757	1.024	.214	.217	.219	.219	.219	.217	.225	.219	.292	.165	.172
18	1.040	9.560	1.386	1.004	1.046	.235	.237	.237	.239	.241	.237	.242	.241	.239	.237	.230
19	1.040	10.160	1.474	.891	1.020	.189	.198	.200	.201	.198	.197	.219	.196	.196	.171	.165
Attached flow, low Reynolds number																
20	0	2.410	0.350	0.217	1.051	0.653	0.642	0.659	0.660	0.659	0.644	0.652	0.656	0.143	0.140	0.137
21	.006	2.220	.322	.213	1.032	.651	.638	.658	.656	.656	.641	.647	.656	.133	.136	.129
22	.012	2.460	.356	.196	1.015	.632	.624	.635	.635	.636	.621	.629	.633	.126	.122	.097
23	.024	2.320	.337	.216	1.025	.590	.584	.595	.597	.598	.583	.589	.596	.122	.127	.127
24	.073	2.230	.323	.303	1.037	.525	.522	.532	.531	.532	.520	.526	.523	.164	.156	.153
25	.150	2.300	.334	.441	1.021	.387	.387	.388	.388	.388	.376	.386	.380	.177	.167	.174
26	.290	2.340	.339	.667	1.041	.272	.274	.275	.272	.271	.261	.268	.253	.205	.178	.179
27	.016	2.270	.329	.218	1.052	.669	.660	.672	.674	.674	.657	.667	.671	.146	.145	.137
28	.032	2.340	.339	.253	1.037	.617	.615	.625	.628	.645	.612	.619	.618	.156	.155	.155
29	.160	2.380	.345	.483	1.036	.330	.331	.331	.332	.331	.326	.330	.328	.171	.157	.179
30	.280	2.460	.356	.617	1.024	.260	.263	.263	.264	.262	.255	.262	.259	.189	.164	.193
31	.540	2.370	.344	.929	1.023	.271	.277	.279	.275	.274	.267	.274	.274	.265	.249	.224
32	.540	2.330	.338	.796	1.028	.213	.218	.219	.218	.216	.211	.217	.211	.191	.172	.129
33	.540	2.430	.353	.751	1.031	.203	.210	.211	.209	.209	.206	.210	.200	.177	.154	.164
34	1.040	2.290	.332	.976	1.047	.244	.249	.249	.250	.249	.243	.249	.246	.246	.244	.287
35	1.040	2.470	.349	.867	1.007	.188	.198	.200	.199	.195	.192	.203	.190	.188	.170	.153
36	1.040	3.180	.461	.842	1.032	.194	.203	.202	.203	.195	.192	.211	.190	.192	.165	.170
37	1.040	4.210	.611	.851	1.043	.193	.203	.204	.203	.199	.191	.218	.194	.194	.165	.166

TABLE III.- Continued

Test	A_l/A_e	Pref		$p_{14}/\bar{p}$	Wing	Cove								Bulkhead	Cavity	
		kPa	psia		p_1/p_{ref}	p_3/p_{ref}	p_4/p_{ref}	p_5/p_{ref}	p_6/p_{ref}	p_7/p_{ref}	p_8/p_{ref}	p_9/p_{ref}	p_{10}/p_{ref}	p_c/p_{ref}	p_{14}/p_{ref}	p_{31}/p_{ref}
Separated flow (a)																
38	0	11.550	1.676	0.027	0.878	1.166	1.188	1.210	1.230	1.238	1.238	1.257	1.258	0.033	0.032	0.031
39	0	1.580	.229	.072	.888	1.301	1.352	1.423	1.480	1.526	1.528	1.596	1.630	.102	.103	.106
40	1.040	1.630	.231	.394	.933	1.082	1.066	1.060	1.036	1.007	.960	1.158	.948	.712	.403	.286
[b]41	1.040	18.690	2.711	.517	.914	.858	.890	.855	.837	.776	.733	1.060	.801	.776	.429	.220
[c]41	1.040	27.970	4.057	.419	-----	.899	1.038	-----	-----	.883	-----	-----	.914	.922	.389	.251
Separated flow (d)																
38	0	2.410	[e]0.350	-----	4.208	5.690	5.700	5.800	5.890	5.930	5.930	6.025	6.030	0.156	0.155	0.149
39	0	.830	[f].120	-----	1.698	2.486	2.583	2.720	2.828	2.916	2.919	3.050	3.115	.195	.197	.203
40	1.040	.830	[f].120	-----	1.802	2.090	2.060	2.051	2.000	1.948	1.854	2.239	1.833	1.375	.779	.552
[b]41	1.040	4.550	[f].660	-----	3.754	3.523	3.652	3.513	3.431	3.183	3.008	4.354	3.288	3.186	1.759	.905
[c]41	1.040	10.160	[g]1.474	-----	-----	2.475	2.858	-----	-----	2.431	-----	-----	2.517	2.538	1.070	.692

[a]Pressures referenced to separated-flow wing pressure.
[b]Data obtained at $\alpha = 5^o$.
[c]Data obtained at $\alpha = 12^o$.
[d]Pressures referenced to attached-flow wing pressure.
[e]$(p_{ref})_{att}$ from test 20.
[f]$(p_{ref})_{att}$ from reference 8.
[g]$(p_{ref})_{att}$ from test 19.

TABLE III.- Continued

Test	Elevon base	Elevon														
	P30/Pref	P15/Pref	P16/Pref	P17/Pref	P18/Pref	P19/Pref	P20/Pref	P21/Pref	P22/Pref	P23/Pref	P24/Pref	P25/Pref	P26/Pref	P27/Pref	P28/Pref	P29/Pref
Attached flow, high Reynolds number																
1	0.333	0.585	0.584	0.588	0.611	0.578	0.612	0.568	2.039	1.366	1.169	1.149	1.119	1.228	1.068	1.133
2	.107	.554	.557	.553	.571	.550	.554	.546	.536	1.893	2.243	2.861	3.258	3.492	3.299	3.812
3	.098	.550	.548	.550	.547	.550	.555	.543	.510	1.271	-----	4.517	-----	5.676	5.435	6.172
4	.156	.566	.565	.565	.576	.560	.565	.559	1.293	1.701	1.616	1.778	1.859	-----	1.861	2.063
5	.108	.566	.573	.565	.583	.563	.567	.565	.527	1.864	1.908	2.803	3.069	3.296	3.251	3.632
6	.128	.566	.562	.565	.571	.562	.551	564	.530	1.878	2.285	2.785	3.046	3.323	3.295	3.524
7	.118	.550	.552	.548	.533	.544	.540	.544	.535	1.958	2.354	2.799	3.082	3.311	3.247	3.497
8	.134	.514	.511	.514	.508	.509	.502	.507	.497	1.886	2.325	2.740	2.932	3.184	3.188	3.505
9	.132	.437	.443	.438	.453	.434	.427	.432	.546	2.027	2.371	2.862	2.976	3.242	3.267	3.508
10	.132	.308	.296	.308	.311	.305	.300	.301	.573	1.899	2.169	2.643	2.755	3.017	3.047	3.279
11	.141	.241	.244	.243	.243	.243	.241	.235	1.003	2.004	2.345	2.600	2.881	3.114	3.113	3.409
12	.127	.528	.519	.530	.528	.528	.519	.528	.536	1.917	2.270	2.596	2.707	2.986	2.968	3.289
13	.144	.498	.490	.497	.508	.495	.488	.495	.547	1.897	2.101	2.493	2.678	2.906	2.860	3.161
14	.133	.263	.260	.262	.255	.263	.257	.257	.861	1.953	2.152	2.726	2.896	3.120	3.091	3.334
15	.148	.236	.235	.236	.242	.235	.232	.228	1.086	1.934	2.199	2.540	2.854	3.076	3.004	3.293
16	.209	.232	.238	.231	.227	.228	.225	.203	2.021	1.703	1.644	1.705	1.760	1.876	1.836	2.004
17	.158	.219	.227	.219	.217	.223	.214	.197	1.191	1.921	2.192	2.610	2.783	3.021	3.012	3.381
18	.229	.239	.245	.240	.234	.235	.233	.208	2.086	1.687	1.651	1.778	1.782	1.881	1.878	2.027
19	.168	.190	.194	.197	.179	.194	.186	.145	1.308	1.810	2.228	2.630	2.919	2.862	3.115	3.514
Attached flow, low Reynolds number																
20	0.142	0.662	0.672	0.658	0.643	0.650	0.649	0.534	0.608	1.631	1.173	2.712	3.085	3.360	3.532	3.528
21	.136	.658	.645	.657	.705	.644	.643	.516	.569	1.719	2.198	2.648	2.988	3.283	3.292	3.447
22	.126	.634	.611	.626	.577	.630	.627	.549	.634	1.817	2.597	3.104	3.103	3.453	3.260	3.481
23	.133	.597	.605	.601	.589	.594	.580	.516	.608	1.757	2.374	2.701	2.899	3.276	3.135	3.581
24	.150	.531	.496	.533	.516	.528	.519	.464	.446	2.021	2.439	2.784	3.045	3.326	3.222	3.439
25	.156	.386	.371	.386	.439	.388	.385	.304	.330	1.971	2.187	2.509	2.837	3.112	3.137	3.309
26	.158	.265	.277	.272	.242	.273	.274	.256	.704	1.941	2.359	2.662	2.973	3.270	3.199	3.364
27	.145	.673	.687	.674	.706	.671	.665	.598	.601	1.747	2.273	2.760	3.105	3.459	3.582	3.494
28	.155	.628	.572	.623	.631	.620	.607	.517	-----	1.760	2.194	2.534	2.828	-----	-----	3.221
29	.156	.331	.311	.336	.306	.333	.326	.287	.464	1.968	-----	2.730	3.099	3.322	3.299	3.360
30	.164	.262	.256	.267	.350	.263	.263	.241	.656	1.856	1.990	2.487	2.728	3.007	3.106	3.098
31	.234	.271	.315	.275	.196	.277	.269	.233	2.126	1.693	1.839	1.717	1.809	1.981	1.778	2.005
32	.173	.214	.227	.224	-----	.218	.210	.211	1.021	1.954	2.457	2.632	2.995	3.280	3.139	3.342
33	.154	.206	.203	.212	.170	.208	.207	.204	.419	2.030	2.812	3.134	3.575	3.925	3.798	4.054
34	.236	.249	.239	.251	.325	.249	.244	.218	2.086	1.676	1.490	1.712	1.729	1.882	1.954	1.964
35	.170	.191	.196	.200	.205	.201	.192	.191	1.121	1.886	1.995	2.523	2.862	3.160	3.110	3.333
36	-----	.189	.204	.203	.176	.199	.194	.184	1.342	1.856	2.164	2.609	2.917	3.223	3.225	3.453
37	.161	.189	.176	.202	.181	.199	.190	.168	1.559	1.806	2.206	2.690	2.987	3.223	3.256	3.383

TABLE III.- Concluded

Test	Elevon base	Elevon														
	P30/Pref	P15/Pref	P16/Pref	P17/Pref	P18/Pref	P19/Pref	P20/Pref	P21/Pref	P22/Pref	P23/Pref	P24/Pref	P25/Pref	P26/Pref	P27/Pref	P28/Pref	P29/Pref
Separated flow (a)																
38	0.035	1 252	1.234	1.223	1.255	1.196	1.163	1.146	-----	-----	-----	-----	-----	-----	-----	-----
39	.106	1.527	1.490	1.469	1.505	1.351	1.286	1.096	-----	-----	-----	-----	-----	-----	-----	-----
40	.236	.921	1.000	.992	1.031	1.035	1.038	.991	-----	-----	-----	-----	-----	-----	-----	-----
[b]41	.171	.692	.753	.802	.830	.831	.815	.873	-----	-----	-----	-----	-----	-----	-----	-----
[c]41	.189	-----	.840	-----	.973	.976	.908	-----	-----	-----	-----	-----	-----	-----	-----	-----
Separated flow (d)																
38	0.167	6.000	5.910	5.870	6.010	5.730	5.575	5.500	-----	-----	-----	-----	-----	-----	-----	-----
39	.203	2.918	2.848	2.808	2.877	2.581	2.457	2.095	-----	-----	-----	-----	-----	-----	-----	-----
40	.455	1.779	1 933	1.918	1.992	2.001	2.007	1.914	-----	-----	-----	-----	-----	-----	-----	-----
[b]41	.704	2.838	3.094	3 292	3.412	3.405	3.345	3.580	-----	-----	-----	-----	-----	-----	-----	-----
[c]41	.521	-----	2.314	-----	2.680	2.688	2.499	-----	-----	-----	-----	-----	-----	-----	-----	-----

[a]Pressures referenced to separated-flow wing pressure.
[b]Data obtained at $\alpha = 5^{o}$.
[c]Data obtained at $\alpha = 12^{o}$.
[d]Pressures referenced to attached-flow wing pressure.

TABLE IV.- NORMALIZED COLD-WALL HEATING RATES

[Normalized values are rounded to three decimal places]

Test	A_l/A_e	$\dot{q}_{ref}$		Wing	Cove								Rub surface		
		kW/m^2	Btu/ft^2-sec	$\dot{q}_1/\dot{q}_{ref}$	$\dot{q}_3/\dot{q}_{ref}$	$\dot{q}_4/\dot{q}_{ref}$	$\dot{q}_5/\dot{q}_{ref}$	$\dot{q}_6/\dot{q}_{ref}$	$\dot{q}_7/\dot{q}_{ref}$	$\dot{q}_8/\dot{q}_{ref}$	$\dot{q}_9/\dot{q}_{ref}$	$\dot{q}_{10}/\dot{q}_{ref}$	$\dot{q}_{11}/\dot{q}_{ref}$	$\dot{q}_{12}/\dot{q}_{ref}$	$\dot{q}_{13}/\dot{q}_{ref}$
Attached flow, high Reynolds number															
1	0	177	15.633	-----	0	-----	0	0	0.003	0.004	0	0.002	0.003	0	0.006
2	0	181	15.974	1.014	0	0.009	0	0	0	0	.002	0	0	0	.001
3	0	139	12.208	1.035	0	.007	0	.001	.001	.002	0	0	0	.001	0
4	0	188	16.579	1.006	0	.017	0	.004	0	.001	.002	.001	0	.004	0
5	0	221	19.469	1.020	.020	.007	.006	.001	.003	.001	.001	.002	.001	.001	.001
6	.006	197	17.367	1.037	.029	.013	.007	.005	.002	.002	.002	.002	.004	.003	.001
7	.012	187	16.500	1.009	.040	.022	.010	.006	.004	.004	.001	.002	.002	.003	.001
8	.024	180	15.889	1.067	.053	.027	.014	.012	.010	.005	.004	.004	.004	.006	.002
9	.073	187	16.500	1.043	.077	.036	.025	.019	.021	.012	.021	.014	.018	.022	.009
10	.150	208	18.336	1.057	.096	.042	.030	.026	.028	.020	.021	.018	.022	.019	.016
11	.290	181	15.909	1.016	.116	.055	.019	.027	.029	.024	.035	.031	.012	.027	.018
12	.016	186	16.342	1.024	.020	.016	.009	.003	.002	.001	.003	.008	.002	.006	.002
13	.032	200	17.577	1.039	.063	.024	.018	.012	.006	.004	.006	.005	.001	.003	.004
14	.160	203	17.892	1.022	.111	.043	.022	.027	.030	.023	.013	.013	.025	.029	.011
15	.280	178	15.715	1.062	.127	.046	.021	.026	.033	.028	.043	.022	.029	.031	.018
16	.540	175	15.423	1.004	.111	.036	.023	.022	.027	.019	.035	.015	.022	.020	.017
17	.540	183	16.158	.995	.193	.092	.047	.041	.043	.038	.065	.036	.049	.044	.028
18	1.040	207	18.208	1.029	.109	.031	.018	.023	.026	.021	.034	.017	.011	.018	.011
19	1.040	205	18.050	1.014	.222	.136	.077	.068	.076	.067	.088	.050	.034	.057	.038
Attached flow, low Reynolds number															
20	0	85	7.476	1.130	0.018	0.006	0	0.006	0	0.002	0.002	0	0.002	0	0.003
21	.006	66	5.855	1.043	.029	.012	.002	.002	0	0	.002	0	.002	0	0
22	.012	71	6.273	.718	.031	.020	.009	.002	.005	0	.002	.002	0	0	0
23	.024	67	5.907	1.120	.033	.021	.005	.002	.010	.007	0	0	0	.002	0
24	.073	74	6.509	.992	.047	.024	0	0	.006	.004	.002	.017	0	0	.002
25	.150	71	6.268	1.034	.081	.030	.012	.018	.023	.007	.009	.009	.011	0	.004
26	.290	69	6.116	1.029	.073	.050	.014	.018	.023	.014	.005	.016	0	.007	.004
27	.016	69	6.116	1.042	.021	.014	0	0	0	.009	0	.002	0	0	.006
28	.032	74	6.482	1.021	.024	.011	.004	.007	0	0	0	0	.004	.002	0
29	.160	68	5.960	1.102	.084	.030	.023	.021	.016	.012	0	.014	.009	.007	.002
30	.280	64	5.620	1.034	.089	.032	.017	.012	.017	.020	.007	.012	.007	.007	.011
31	.540	65	5.751	1.019	.092	.027	.012	.017	.034	.017	.019	0	.007	.007	.007
32	.540	77	6.770	1.050	.105	.031	.014	.017	.027	.023	.012	.004	.012	.010	.011
33	.540	72	6.378	1.012	.111	.046	.013	.018	.022	.013	.026	.007	.012	.013	.006
34	1.040	74	6.482	1.034	.084	.019	.013	.013	.022	.013	.006	.002	.006	0	.008
35	1.040	69	6.064	1.016	.173	.099	.060	.053	.044	.039	.058	.030	.013	.028	.015
36	1.040	78	6.848	1.049	.212	.120	.065	.059	.071	.057	.084	.045	.021	.035	.022
37	1.040	91	7.998	1.027	.195	.112	.059	.056	.063	.054	.080	.049	.013	.047	.025

TABLE IV.- Continued

Test	$A_l A_e$	$\dot{q}_{ref}$		Wing	Cove								Rub surface		
		kW/m^2	Btu/ft^2-sec	$\dot{q}_1/\dot{q}_{ref}$	$\dot{q}_3/\dot{q}_{ref}$	$\dot{q}_4/\dot{q}_{ref}$	$\dot{q}_5/\dot{q}_{ref}$	$\dot{q}_6/\dot{q}_{ref}$	$\dot{q}_7/\dot{q}_{ref}$	$\dot{q}_8/\dot{q}_{ref}$	$\dot{q}_9/\dot{q}_{ref}$	$\dot{q}_{10}/\dot{q}_{ref}$	$\dot{q}_{11}/\dot{q}_{ref}$	$\dot{q}_{12}/\dot{q}_{ref}$	$\dot{q}_{13}/\dot{q}_{ref}$
Separated flow (a)															
38	0	141	12.39	0.818	0.624	0.491	0.440	0.385	0.345	0.279	0.365	0.219	0.170	0.120	0.002
39	0	34	3.01	.548	.380	.301	.264	.227	.255	.274	.287	.148	.117	.056	.013
40	1.040	53	4.68	.583	.754	.618	.557	.488	.453	.375	.855	.378	.285	.408	.178
[b]41	1.040	265	23.38	.661	.893	.752	.652	.570	.543	.486	.928	.506	.553	.893	.496
41	1.040	---	-----	-----	-----	-----	-----	-----	-----	-----	-----	-----	-----	-----	-----
Separated flow (c)															
38	0	85	[d]7.48	1.355	1.035	0.813	0.729	0.638	0.572	0.479	0.606	0.364	0.282	0.200	0.003
39	0	19	[e]1.70	.969	.673	.533	.467	.402	.451	.484	.508	.262	.208	.984	.223
40	1.040	19	[e]1.70	1.605	2.075	1.703	1.533	1.345	1.245	1.033	2.360	1.040	.784	1.123	.490
[b]41	1.040	109	[e]9.60	2.436	2.175	1.830	1.588	1.390	1.322	1.184	2.260	1.233	1.350	2.175	1.210

[a]Heating rates referenced to separated-flow wing heating rate.
[b]Data obtained at $\alpha = 5^o$.
[c]Heating rates referenced to attached-flow wing heating rate.
[d]$(\dot{q}_{ref})_{att}$ from test 20.
[e]$(\dot{q}_{ref})_{att}$ from reference 8.

TABLE IV.- Continued

Test	Elevon														
	$\dot{q}_{15}/\dot{q}_{ref}$	$\dot{q}_{16}/\dot{q}_{ref}$	$\dot{q}_{17}/\dot{q}_{ref}$	$\dot{q}_{18}/\dot{q}_{ref}$	$\dot{q}_{19}/\dot{q}_{ref}$	$\dot{q}_{20}/\dot{q}_{ref}$	$\dot{q}_{21}/\dot{q}_{ref}$	$\dot{q}_{22}/\dot{q}_{ref}$	$\dot{q}_{23}/\dot{q}_{ref}$	$\dot{q}_{24}/\dot{q}_{ref}$	$\dot{q}_{25}/\dot{q}_{ref}$	$\dot{q}_{26}/\dot{q}_{ref}$	$\dot{q}_{27}/\dot{q}_{ref}$	$\dot{q}_{28}/\dot{q}_{ref}$	$\dot{q}_{29}/\dot{q}_{ref}$
Attached flow, high Reynolds number															
1	0.006	0.005	0.002	0.005	0.010	0.003	-----	2.262	-----	0.424	0.958	0.948	0.912	0.879	0.973
2	0	0	0	0	0	.008	0.019	.573	2.121	.800	2.168	2.522	2.602	2.639	2.860
3	0	0	0	.004	.004	.004	.017	.103	1.920	1.292	2.433	2.788	2.848	2.826	2.980
4	0	0	.006	.003	.015	.034	.082	2.090	1.808	.651	1.522	1.643	1.662	1.691	1.832
5	.001	.003	.001	.001	.003	.006	.031	.620	1.992	.507	2.038	2.327	2.374	2.399	2.597
6	.004	.001	.003	.004	.016	.031	.044	.718	2.185	-----	2.103	2.261	2.264	2.309	2.475
7	.003	.005	.008	.008	.018	.038	.049	.784	2.283	-----	2.118	2.288	2.283	2.327	2.525
8	.008	.008	.014	.018	.024	.041	.032	.904	2.244	1.060	1.889	2.057	2.090	2.133	2.308
9	.020	.023	.018	.026	.031	.040	.075	1.114	2.198	.165	2.042	2.197	2.267	2.295	2.446
10	.021	.028	.029	.032	.043	.047	.063	1.349	2.039	.232	1.833	1.955	2.007	2.106	3.995
11	.027	.027	.033	.035	.040	.064	.065	1.972	1.740	.533	1.713	1.888	1.922	2.030	2.040
12	.005	.002	.006	.002	.012	.037	.039	.912	2.129	.482	1.918	2.158	2.200	2.156	2.513
13	.004	.006	.013	.019	.026	.036	.058	1.036	2.157	.088	1.904	2.053	2.032	2.074	-----
14	.013	.007	.031	.028	.035	.056	.083	1.710	1.733	.823	1.766	2.042	2.230	2.312	2.192
15	.026	.024	.029	.035	.040	.052	.118	2.274	1.919	.811	1.742	1.891	2.005	2.077	3.770
16	.026	.012	.025	.033	.054	.064	.239	2.319	1.374	.481	1.310	1.370	1.390	1.462	1.687
17	.037	.020	.041	.058	.075	.105	.164	2.430	1.610	.686	1.786	2.028	2.180	2.221	2.424
18	.010	0	.024	.032	.047	.069	.221	2.212	1.309	-----	1.252	1.347	1.406	1.491	1.727
19	.050	-----	.059	.088	.112	.160	.175	2.464	1.539	-----	1.815	2.146	-----	-----	2.628
Attached flow, low Reynolds number															
20	0.007	0.007	0	0.004	0.007	0.004	0.025	0.145	2.151	-----	2.226	2.565	2.570	2.569	2.754
21	0	0	.004	0	.009	.009	.009	.199	2.503	-----	2.471	2.693	2.669	2.705	2.705
22	.004	.004	.016	.008	.012	.008	.024	.258	2.618	-----	2.302	2.695	2.727	2.738	2.929
23	0	.017	.009	0	.004	.026	.026	.265	2.772	1.256	2.382	2.749	2.796	2.791	3.077
24	0	0	.085	.016	0	.016	.066	.505	2.764	1.277	2.177	2.405	2.374	2.391	2.648
25	.008	.013	0	.013	.013	.054	.050	.700	2.517	.027	1.927	2.536	2.565	2.600	2.767
26	.004	.017	.017	.021	.033	.050	.062	1.339	1.991	.606	2.068	2.200	2.274	2.327	2.631
27	0	0	.012	.008	0	.004	.021	.248	2.553	2.512	2.436	2.529	2.559	2.582	2.551
28	0	.004	0	.008	.012	.004	.020	.316	2.431	-----	2.027	2.315	2.265	2.260	-----
29	0	0	.025	.025	.009	.055	.085	1.035	2.162	.695	2.014	2.195	2.211	2.310	2.523
30	0	.014	.023	.023	.014	.054	.076	1.340	1.862	.583	1.874	2.168	2.159	2.254	2.349
31	.004	.070	.004	.009	.053	.062	.132	3.102	1.494	.455	1.088	1.564	1.630	1.642	1.821
32	.019	.019	.011	.011	.045	.082	.049	1.807	1.784	.616	1.994	2.333	2.344	2.370	2.663
33	.016	.008	.044	.036	.020	.071	.071	.844	1.862	.768	2.193	2.691	2.805	2.897	3.156
34	.004	0	.012	.012	.031	.074	.152	2.955	1.458	-----	1.200	1.527	1.554	1.591	1.696
35	.038	.038	.063	.075	.079	.125	.083	2.650	1.525	-----	2.348	2.471	2.529	2.543	2.617
36	.041	.059	.059	.070	.089	.151	.118	3.055	1.520	-----	2.360	2.514	2.567	2.631	2.689
37	.044	.060	.044	.076	.095	.142	.114	2.967	1.497	-----	2.076	2.282	-----	-----	2.601

TABLE IV.- Concluded

Test	Elevon															
	$\dot{q}_{15}/\dot{q}_{ref}$	$\dot{q}_{16}/\dot{q}_{ref}$	$\dot{q}_{17}/\dot{q}_{ref}$	$\dot{q}_{18}/\dot{q}_{ref}$	$\dot{q}_{19}/\dot{q}_{ref}$	$\dot{q}_{20}/\dot{q}_{ref}$	$\dot{q}_{21}/\dot{q}_{ref}$	$\dot{q}_{22}/\dot{q}_{ref}$	$\dot{q}_{23}/\dot{q}_{ref}$	$\dot{q}_{24}/\dot{q}_{ref}$	$\dot{q}_{25}/\dot{q}_{ref}$	$\dot{q}_{26}/\dot{q}_{ref}$	$\dot{q}_{27}/\dot{q}_{ref}$	$\dot{q}_{28}/\dot{q}_{ref}$	$\dot{q}_{29}/\dot{q}_{ref}$
Separated flow (a)																
38	0.234	0.315	0.358	0.369	0.418	0.505	0.865	-----	-----	-----	-----	-----	-----	-----	-----
39	.235	.294	.303	.269	.294	.328	.412	-----	-----	-----	-----	-----	-----	-----	-----
40	.308	.243	.394	.491	.556	.695	1.242	-----	-----	-----	-----	-----	-----	-----	-----
[b]41	.373	.314	.515	.608	.702	.824	1.253	-----	-----	-----	-----	-----	-----	-----	-----
41	-----	-----	-----	-----	-----	-----	-----	-----	-----	-----	-----	-----	-----	-----	-----
Separated flow (c)																
38	0.419	0.565	0.642	0.662	0.750	0.906	1.432	-----	-----	-----	-----	-----	-----	-----	-----
39	.416	.520	.535	.475	.519	.579	.728	-----	-----	-----	-----	-----	-----	-----	-----
40	.846	.668	1.084	1.353	1.528	1.916	3.420	-----	-----	-----	-----	-----	-----	-----	-----
[b]41	.908	.765	1.255	1.480	1.710	2.010	3.050	-----	-----	-----	-----	-----	-----	-----	-----

[a]Heating rates referenced to separated-flow wing heating rate.
[b]Data obtained at $\alpha = 5^{o}$.
[c]Heating rates referenced to attached-flow wing heating rate.

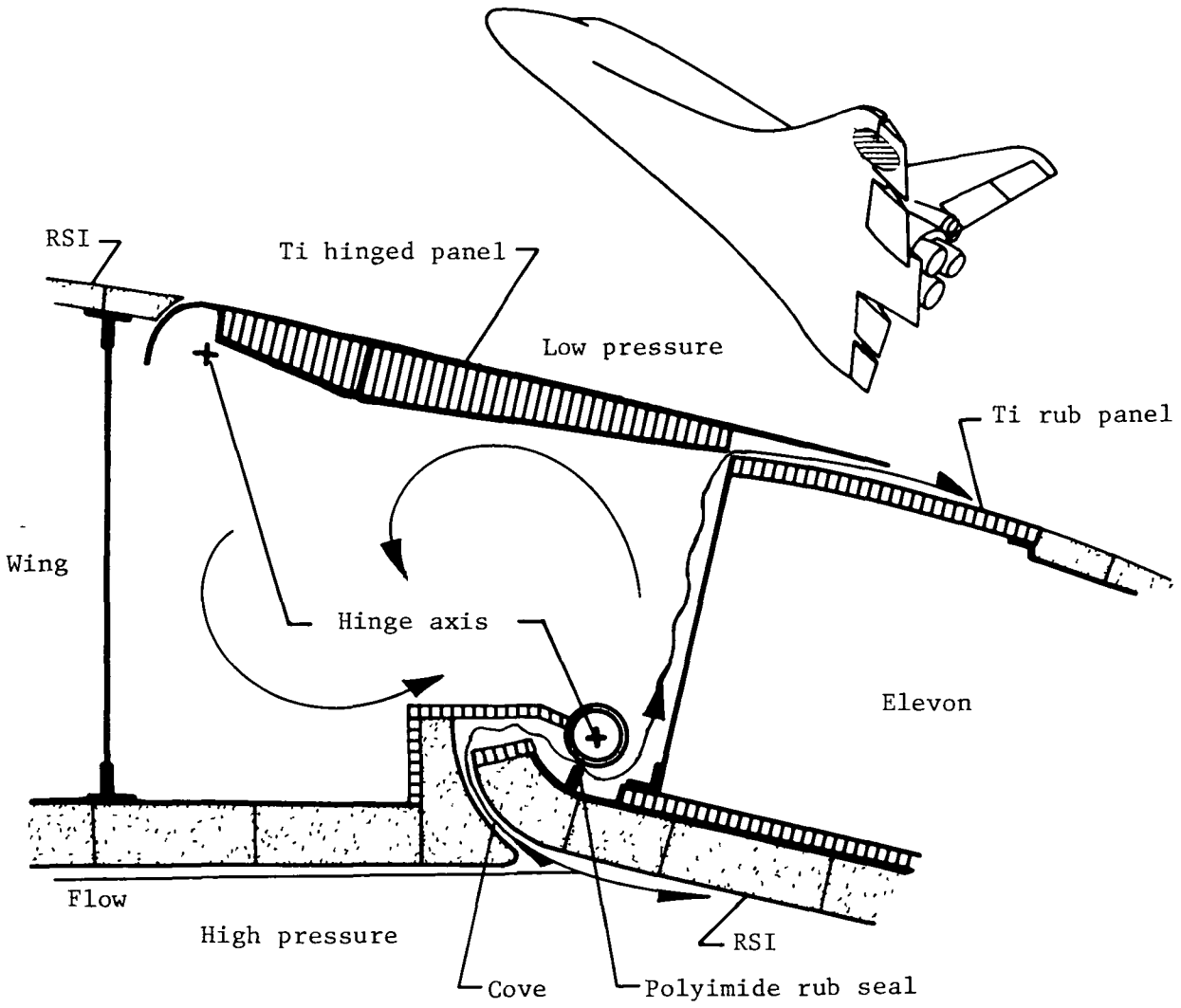

Figure 1.- Cross section of space shuttle orbiter structure at wing-elevon juncture.

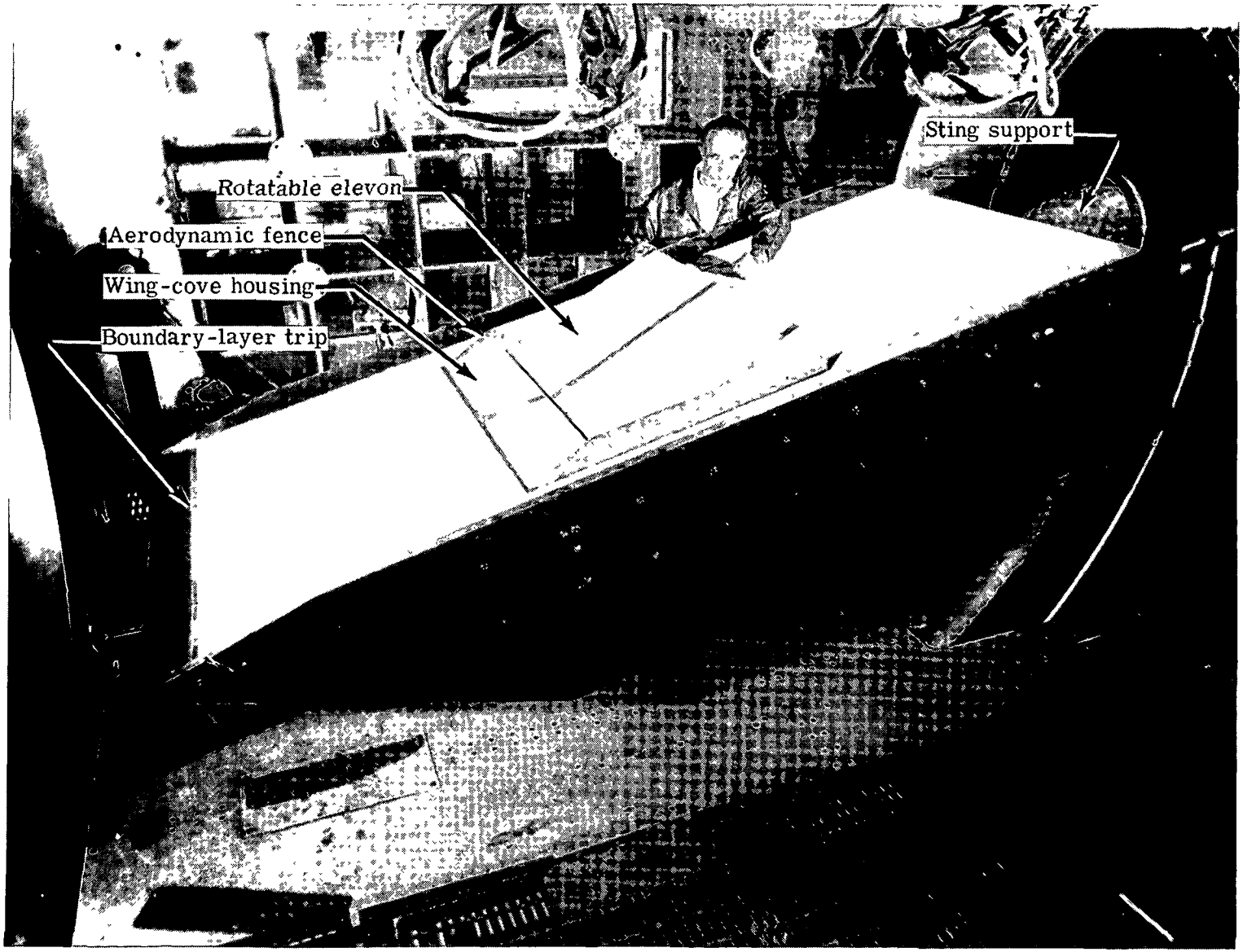

L-76-4512.1

Figure 2.- Test installation.

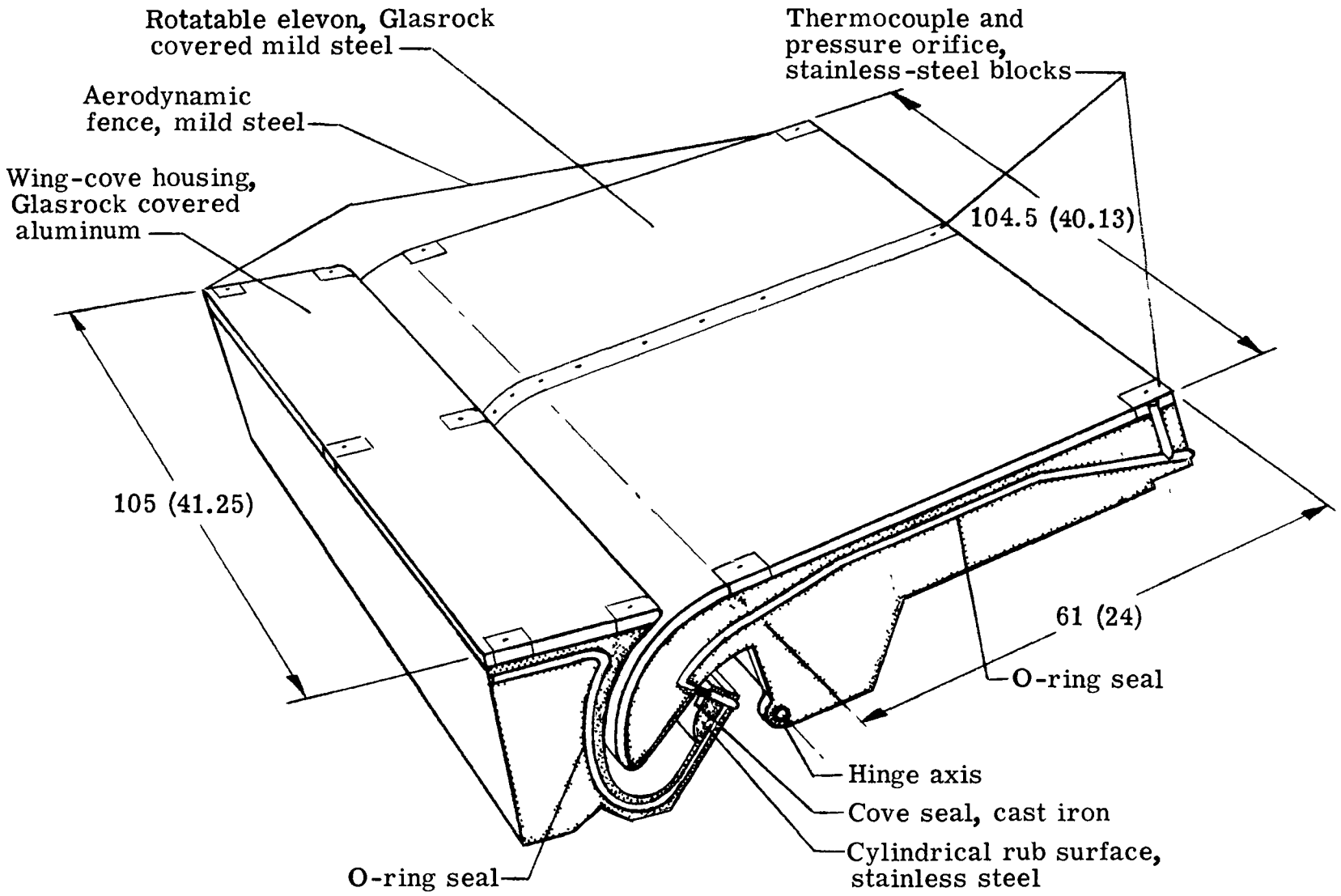

Figure 3.- Illustration of model with one aerodynamic fence removed. Dimensions are in centimeters (inches).

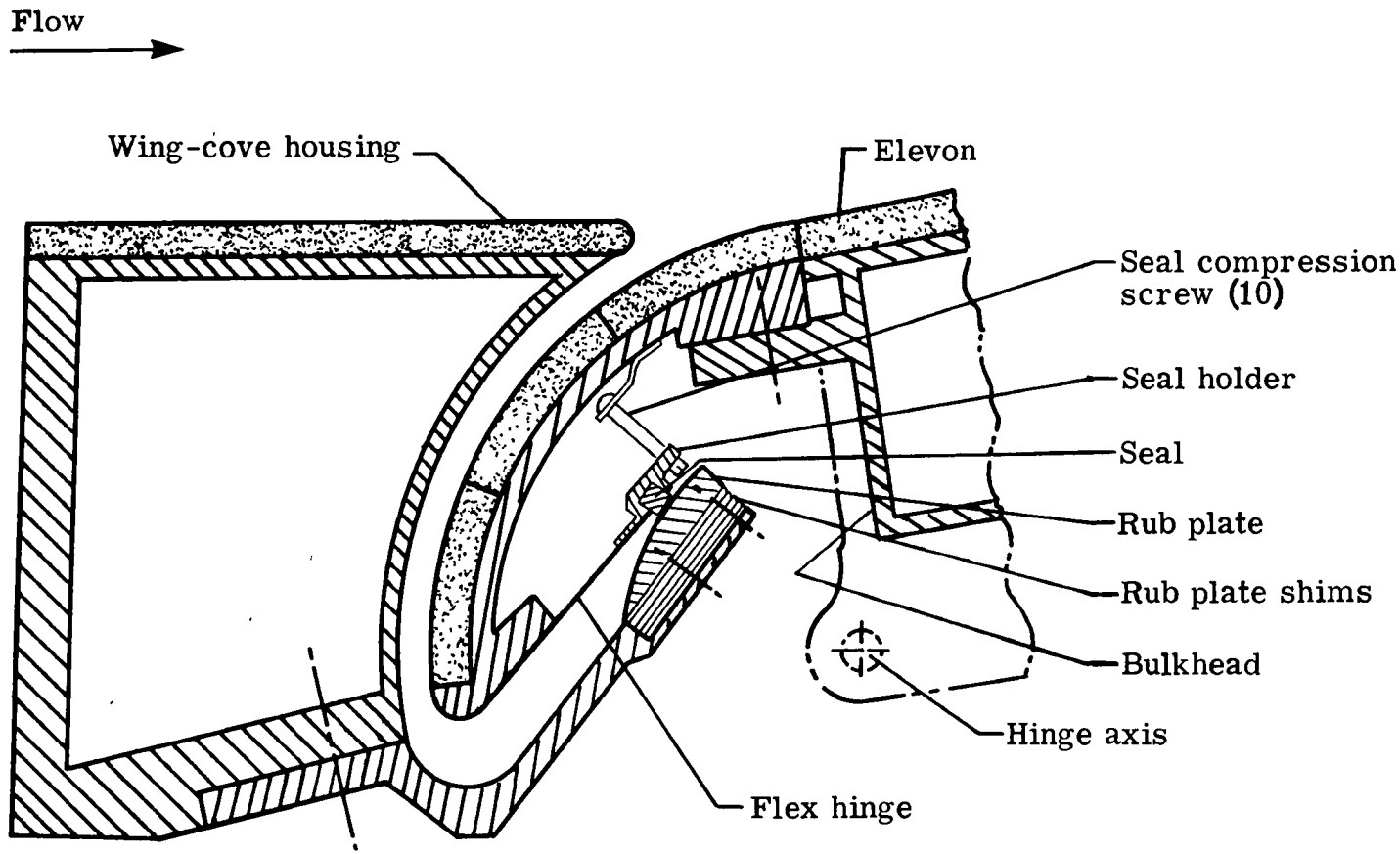

(a) Arrangement of wing-cove housing, elevon, and seal.

Figure 4.- Cross section of model at juncture of wing and elevon.
Dimensions are in centimeters (inches).

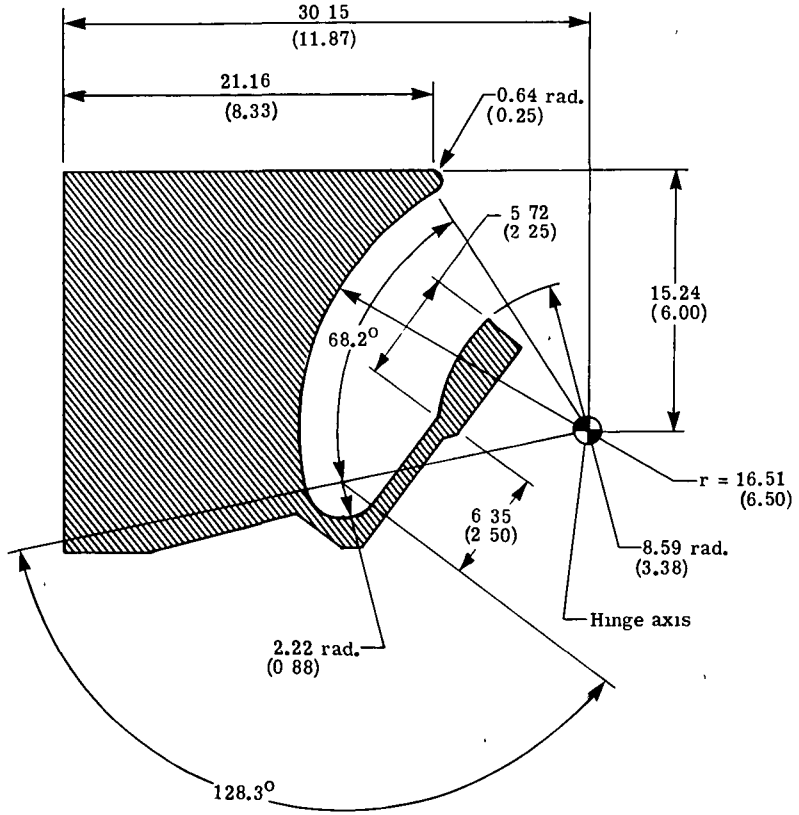

(b) Wing-cove housing.

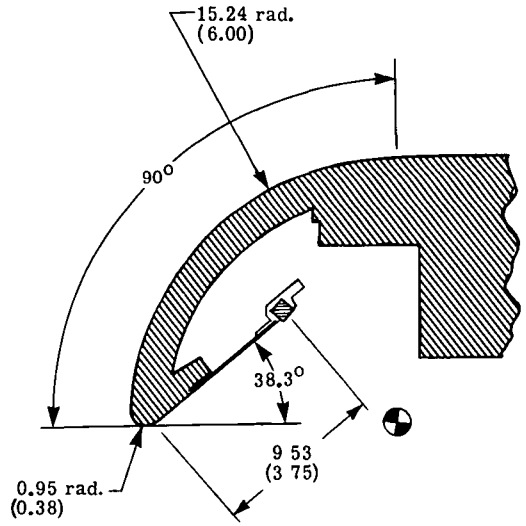

(c) Elevon.

Figure 4.- Concluded.

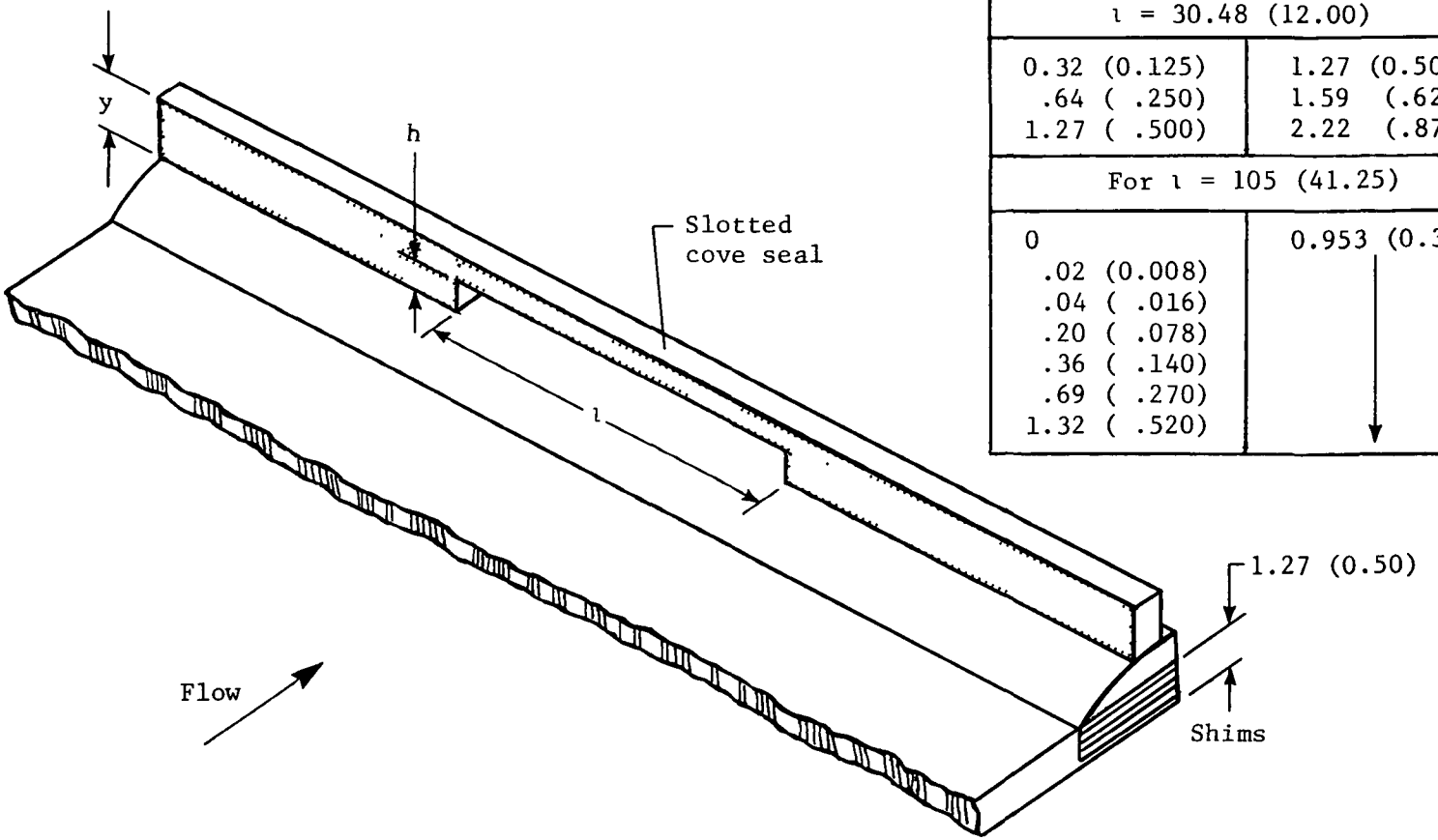

h	y
For l = 2.54 (1.00) and l = 30.48 (12.00)	
0.32 (0.125) .64 (.250) 1.27 (.500)	1.27 (0.500) 1.59 (.625) 2.22 (.875)
For l = 105 (41.25)	
0 .02 (0.008) .04 (.016) .20 (.078) .36 (.140) .69 (.270) 1.32 (.520)	0.953 (0.375)

Figure 5.- Seal and rub surface arrangement.
Dimensions are in centimeters (inches).

Distance from wall for thermocouple at location -		
a	b	c
0.64 (0 25)	0 30 (0.13) 64 (.25) .97 (.38)	0 16 (0 06)

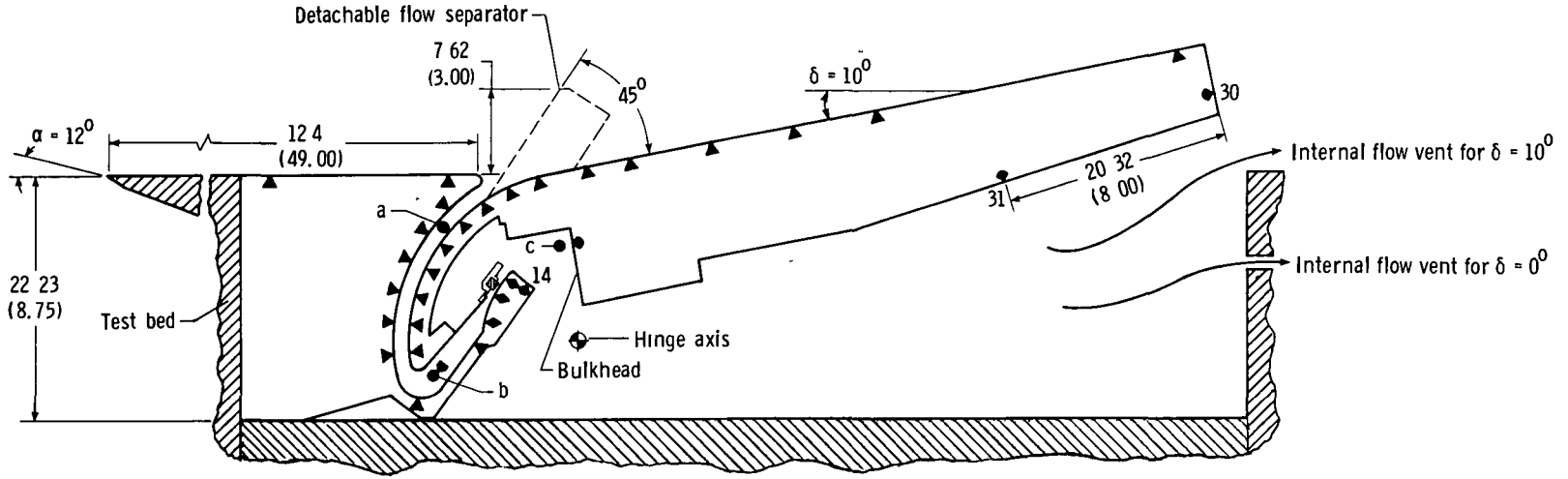

Symbol	Sensors
●	Cove gas thermocouple (5 spanwise at c)
◆	Pitot pressure probe
♦	Wall thermocouple
▲	Wall thermocouple and static pressure orifice
◆	Static pressure orifice (5 spanwise at c)

Figure 6.- Cross section of model installed in test bed and centerline instrumentation distribution. Dimensions are in centimeters (inches).

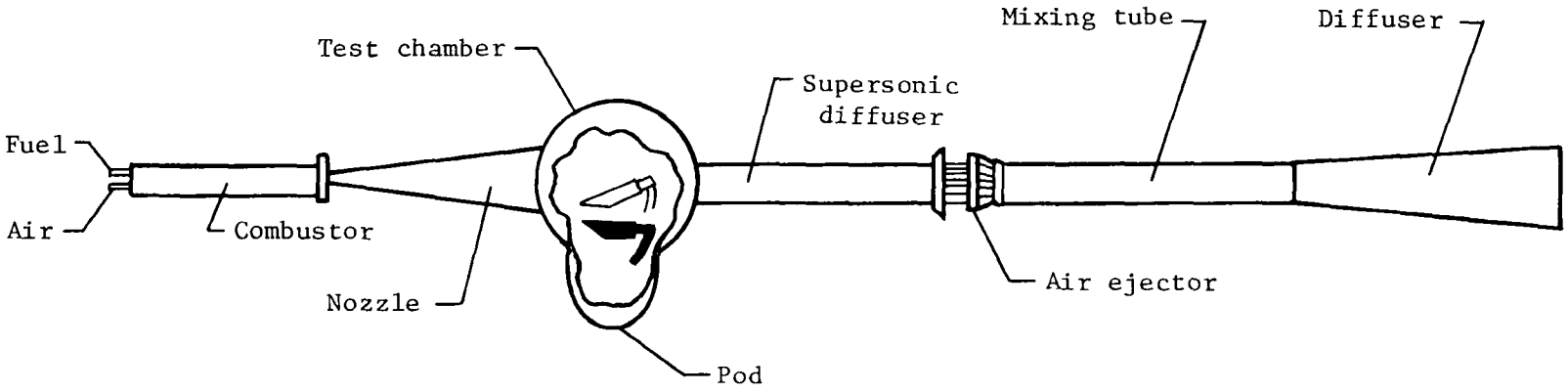

Figure 7.- Schematic of Langley 8-foot high-temperature structures tunnel.

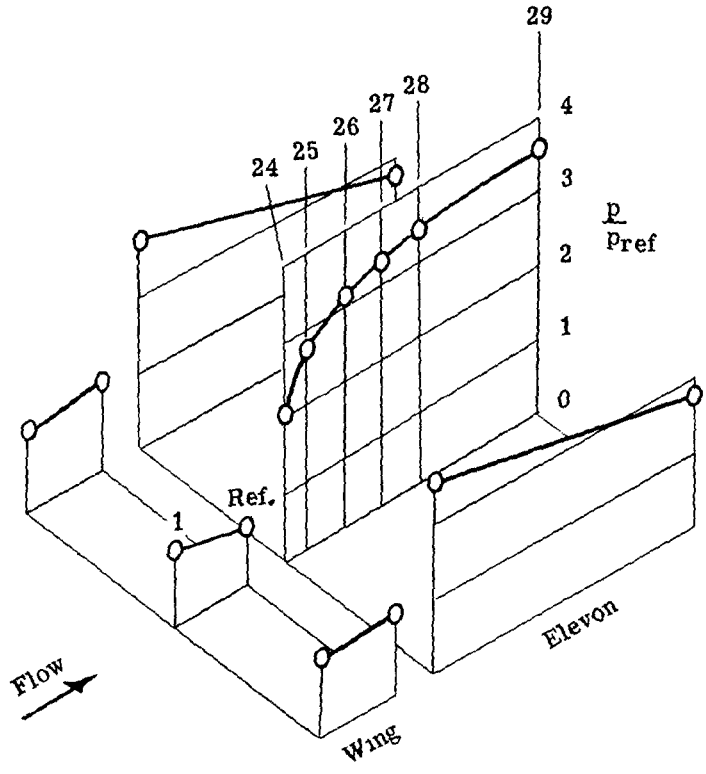

(a) Pressures.

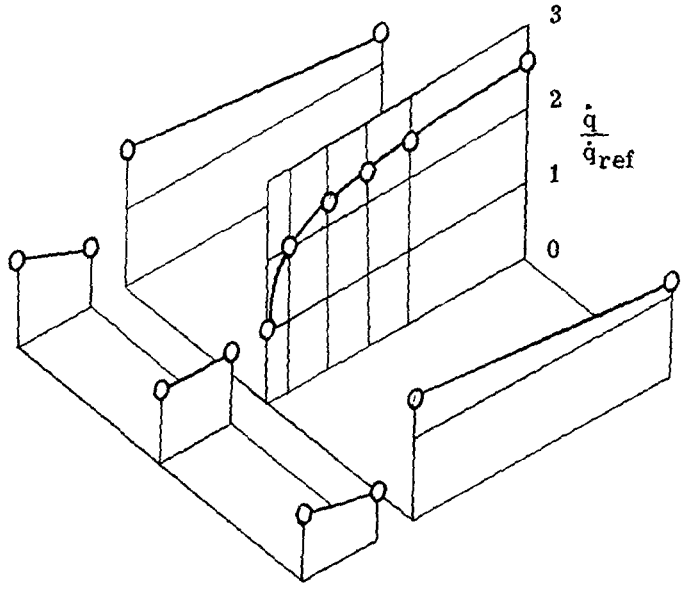

(b) Heating rates.

Figure 8.- Typical pressure and heating-rate distributions on wing and elevon. $R_\infty = 4.40 \times 10^6$ per meter (1.34×10^6 per foot); $T_t = 1888$ K (3400° R); $\alpha = 12^\circ$; $\delta = 10^\circ$.

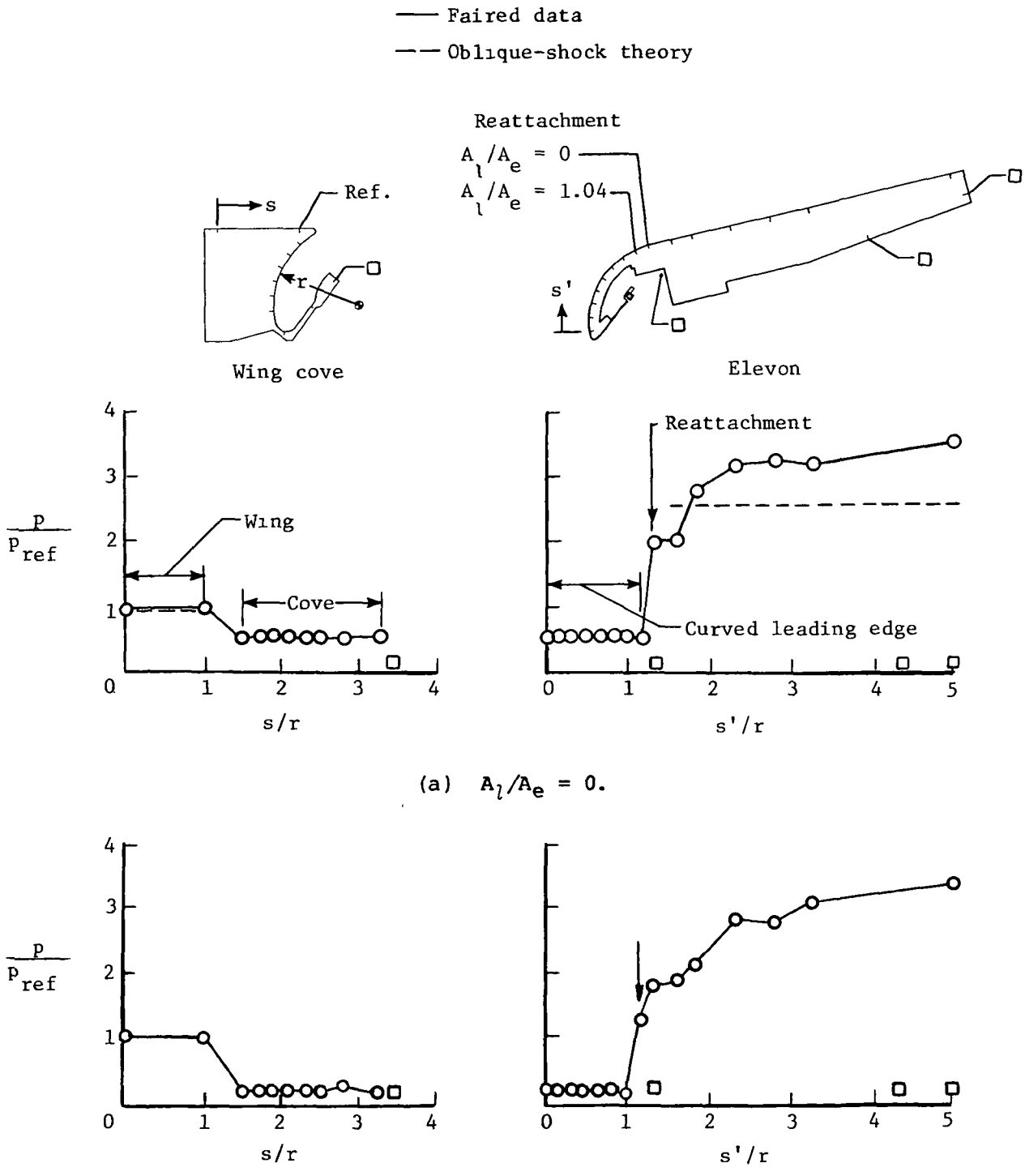

(a) $A_l/A_e = 0$.

(b) $A_l/A_e = 1.04$.

Figure 9.- Centerline pressure distributions for attached flow.
$R_\infty = 4.40 \times 10^6$ per meter (1.34×10^6 per foot);
$T_t = 1888$ K (3400° R); $\alpha = 12°$; $\delta = 10°$.

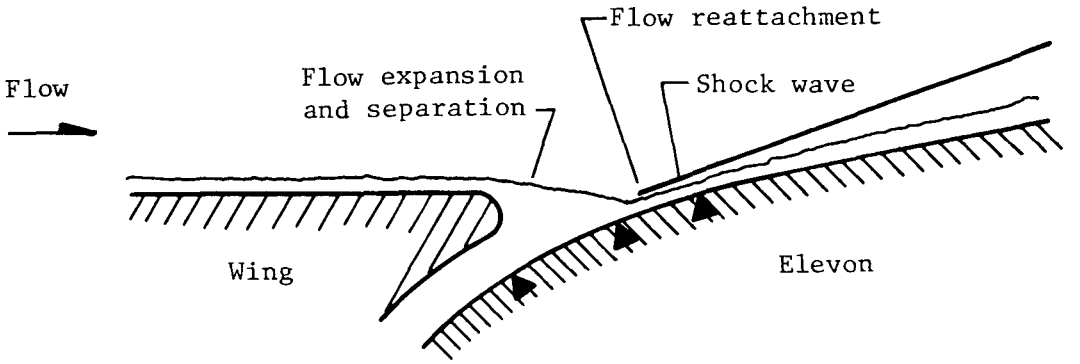

(a) $A_l/A_e = 0.$

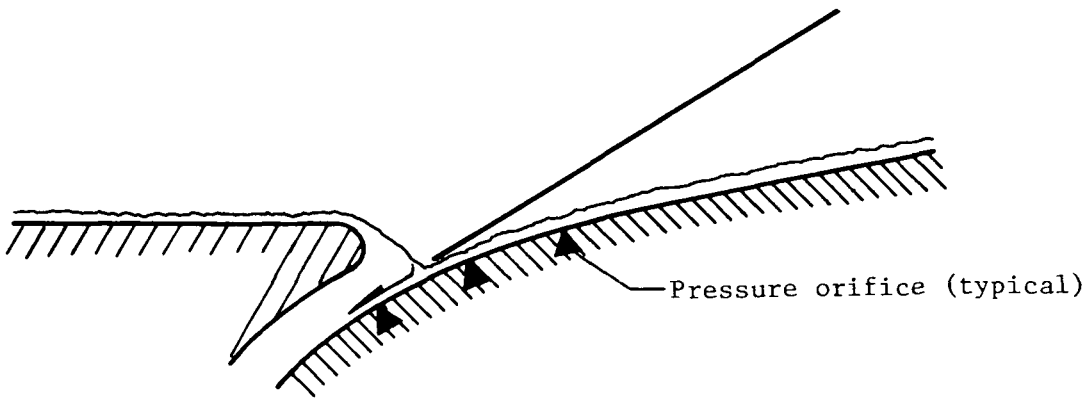

(b) $A_l/A_e = 1.04.$

Figure 10.- Simplified flow details across cove entrance for attached flow.

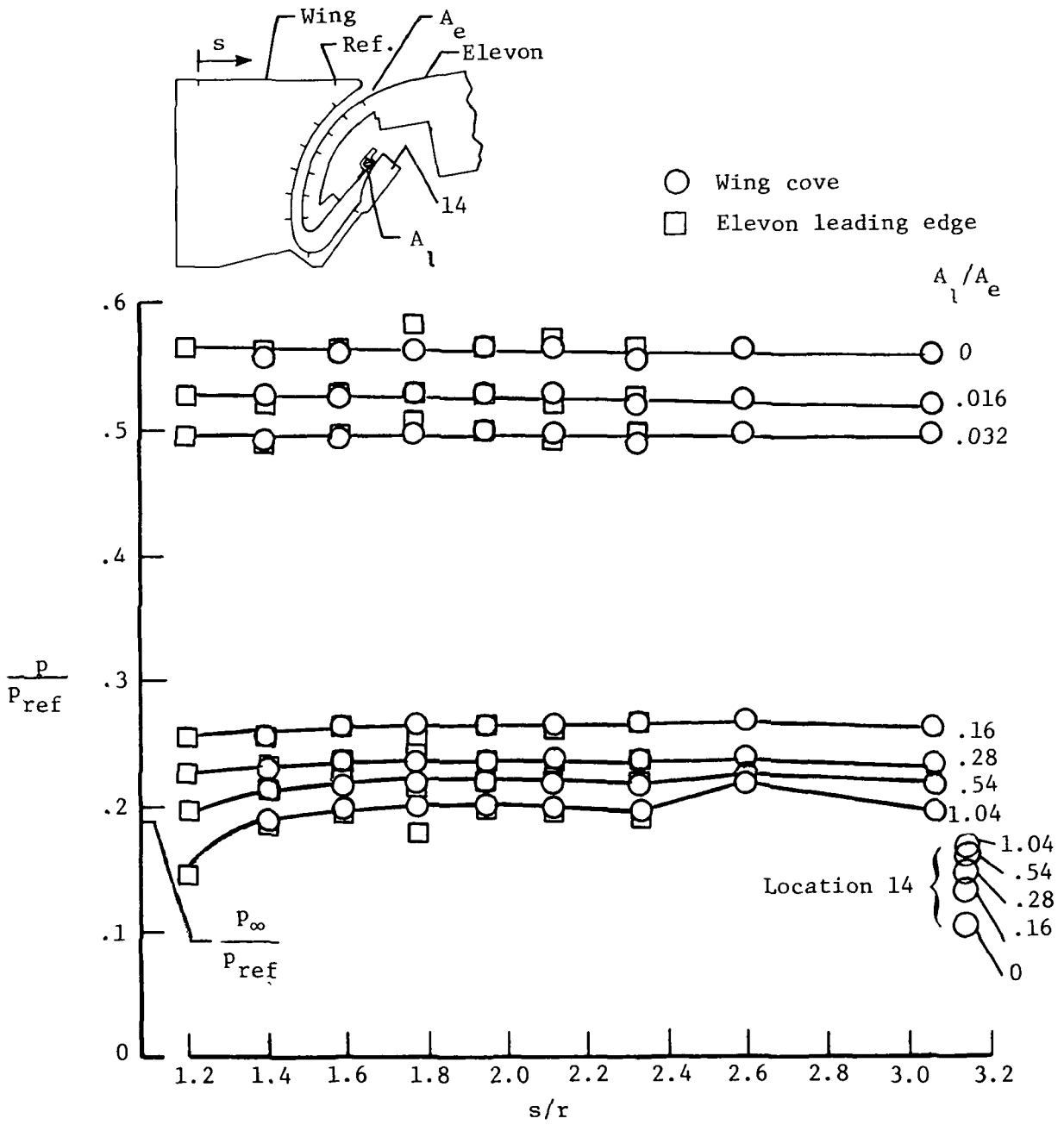

Figure 11.- Cove pressure distributions for full-span leaks. Attached flow; R_∞ = 4.40 × 10^6 per meter (1.34 × 10^6 per foot); T_t = 1888 K (3400° R); α = 12°; δ = 10°.

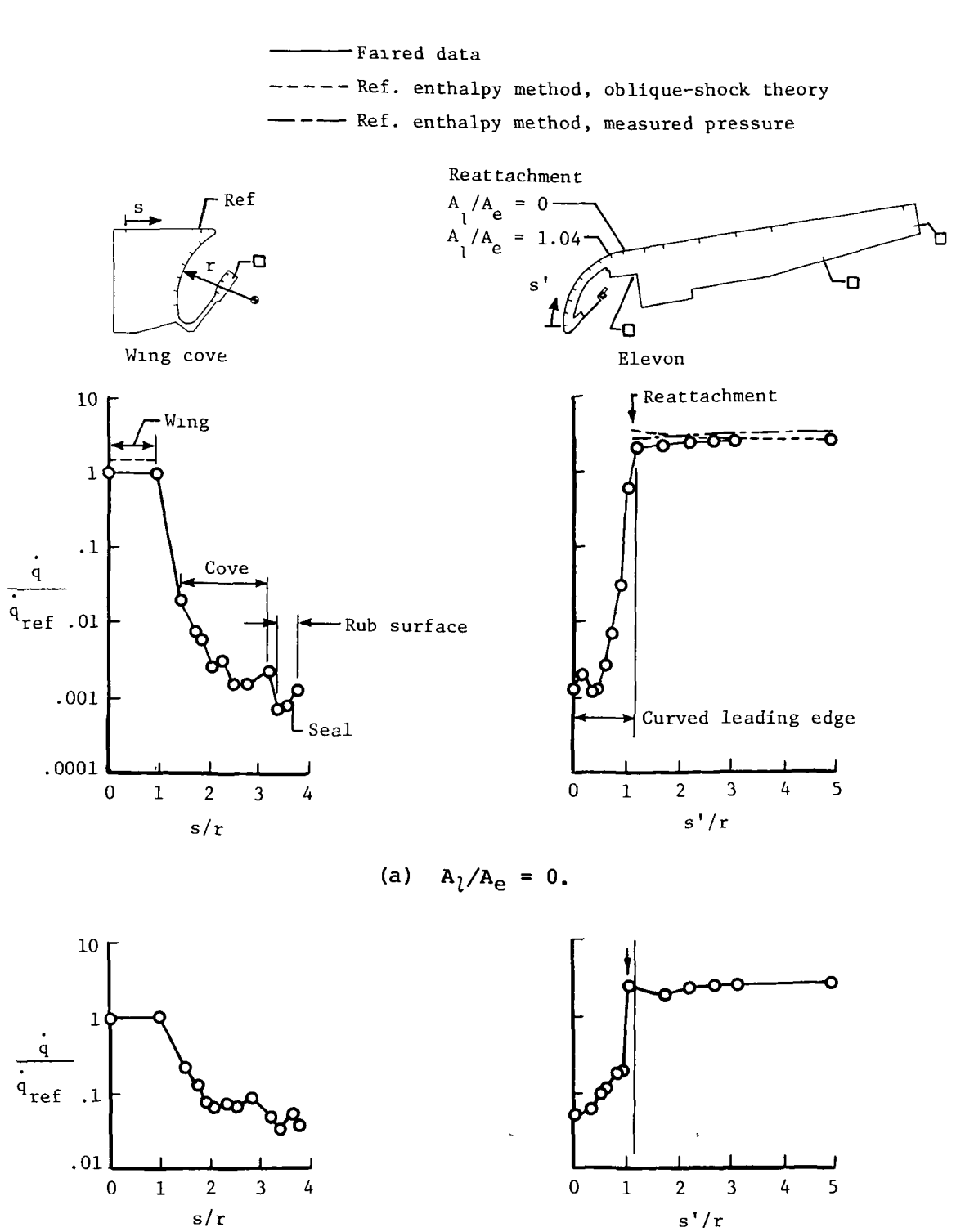

Figure 12.- Centerline cold-wall heating-rate distributions for attached flow. R_∞ = 4.40 × 10^6 per meter (1.34 × 10^6 per foot); T_t = 1888 K (3400° R); α = 12°; δ = 10°.

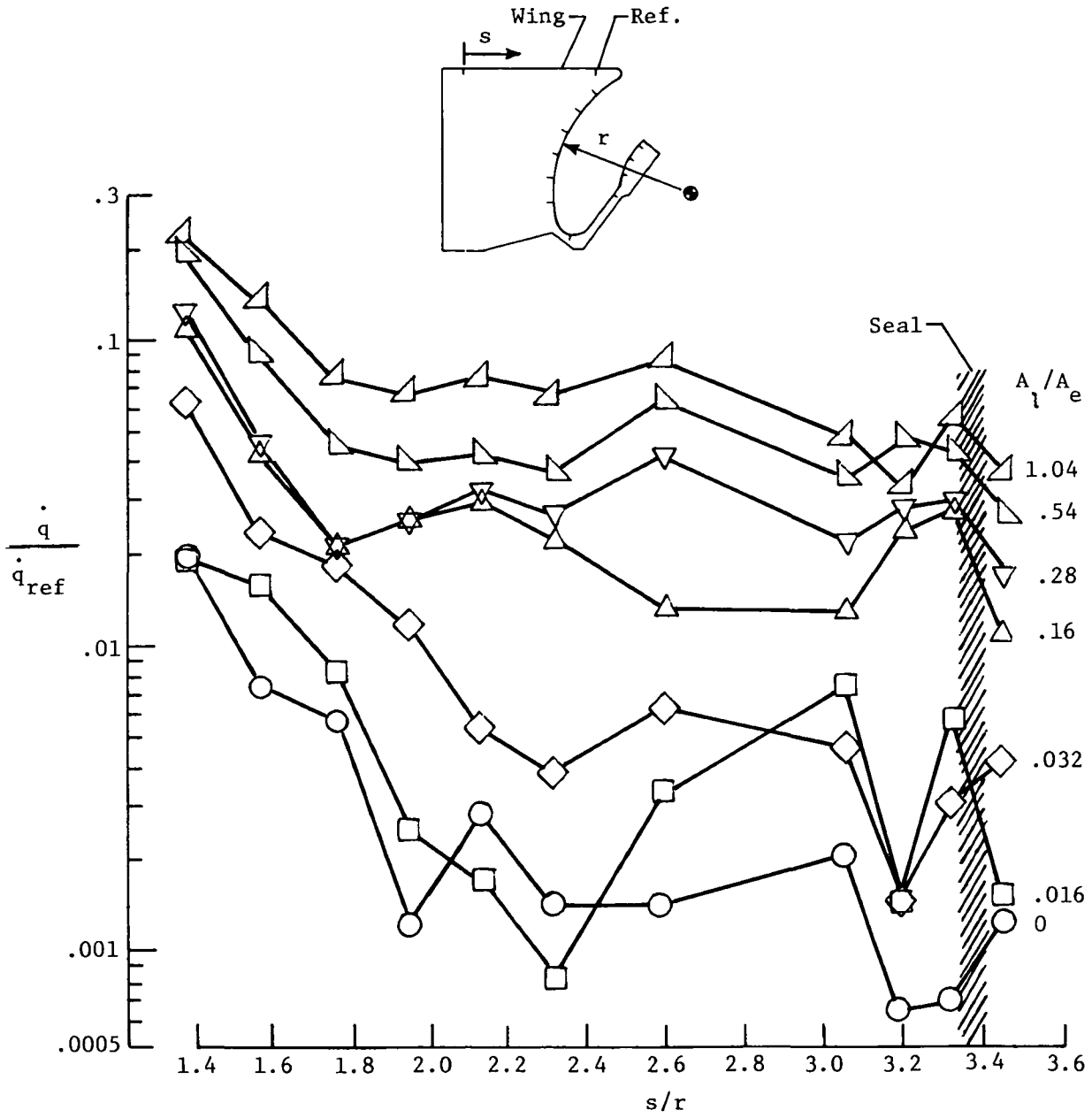

Figure 13.- Cove cold-wall heating-rate distributions for full-span leaks. Attached flow; $R_\infty = 4.40 \times 10^6$ per meter (1.34×10^6 per foot); $T_t = 1888$ K (3400° R); $\alpha = 12^\circ$; $\delta = 10^\circ$.

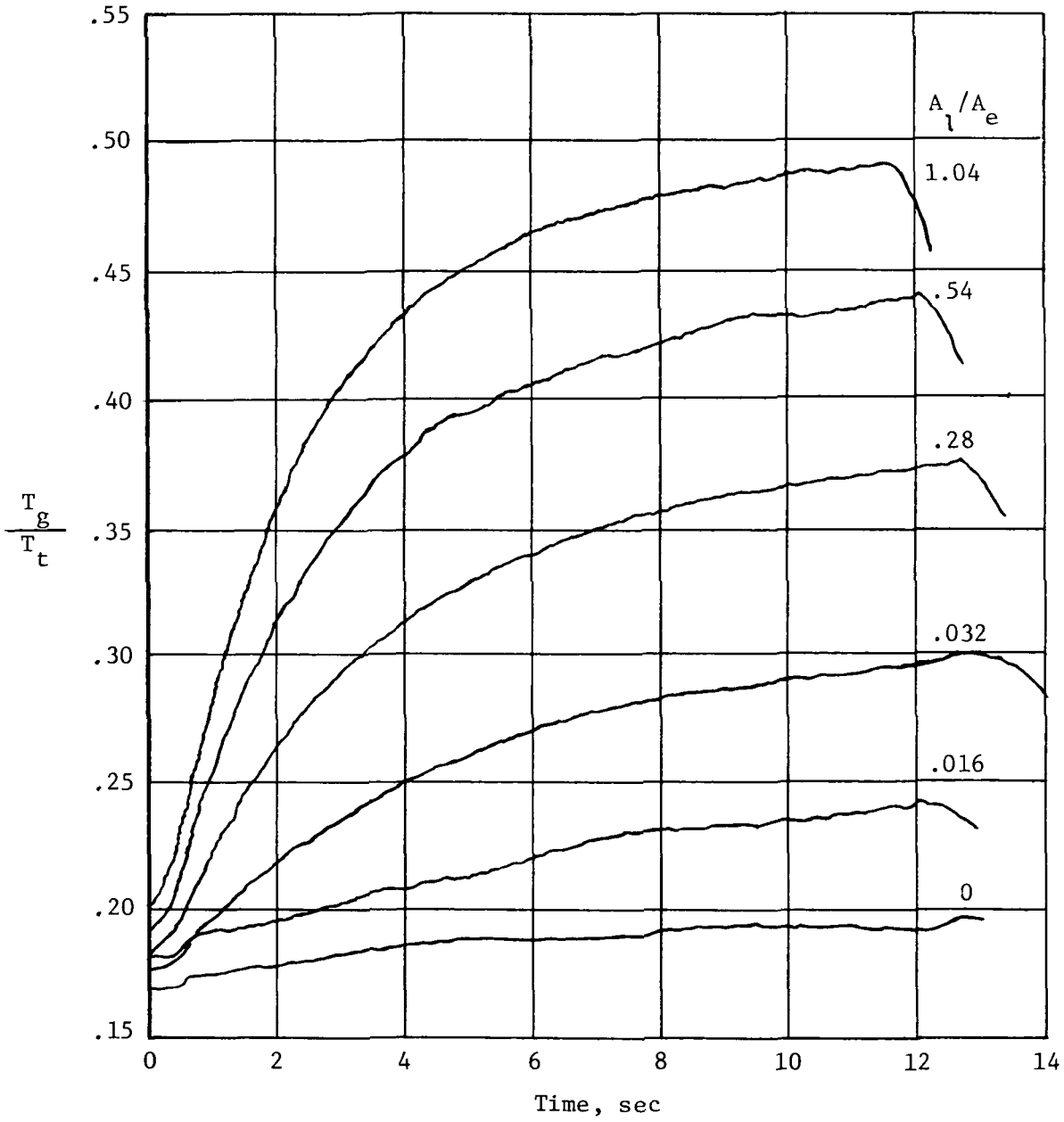

(a) Near cove entrance (location a, fig. 6), 0.64 cm (0.25 in.) from wall.

Figure 14.- Responses of beaded thermocouples located between cove walls for full-span leaks. Attached flow; $R_\infty = 4.40 \times 10^6$ per meter (1.34×10^6 per foot); $T_t = 1888$ K (3400° R); $\alpha = 12^\circ$; $\delta = 10^\circ$.

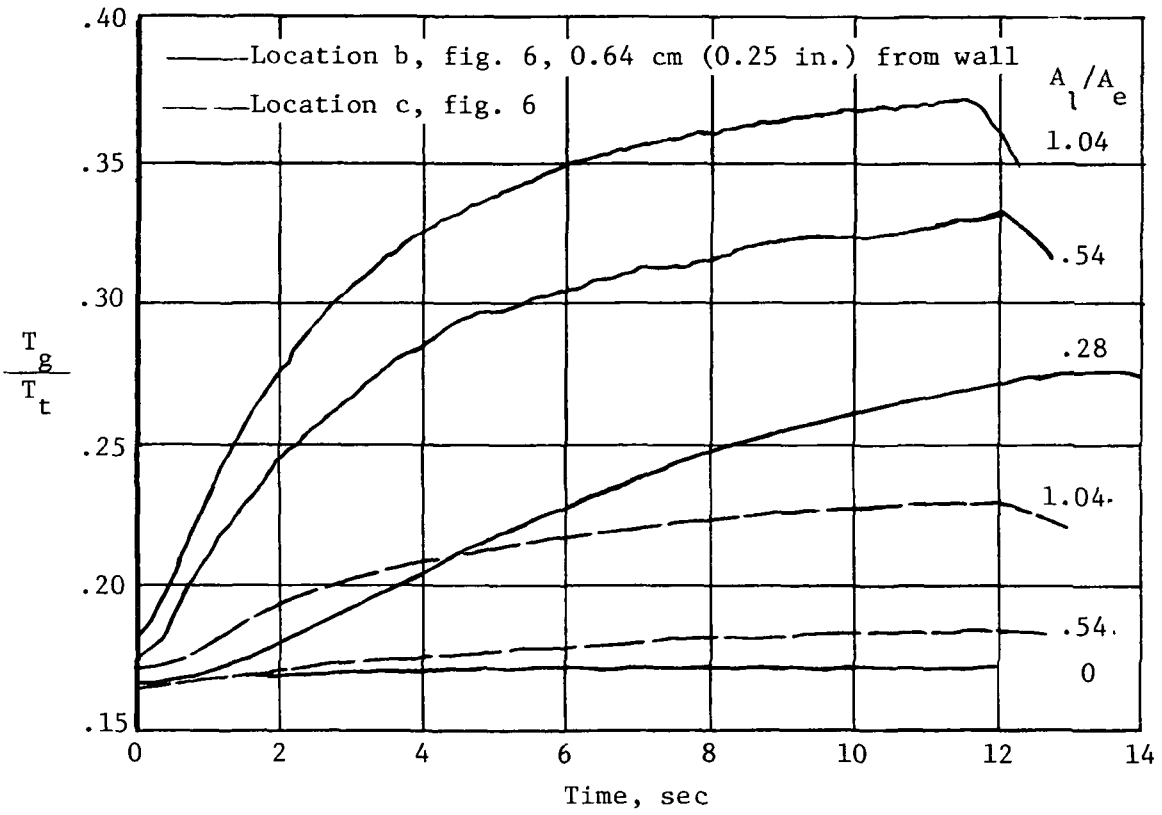

(b) Near cove seal and bulkhead.

Figure 14.- Continued.

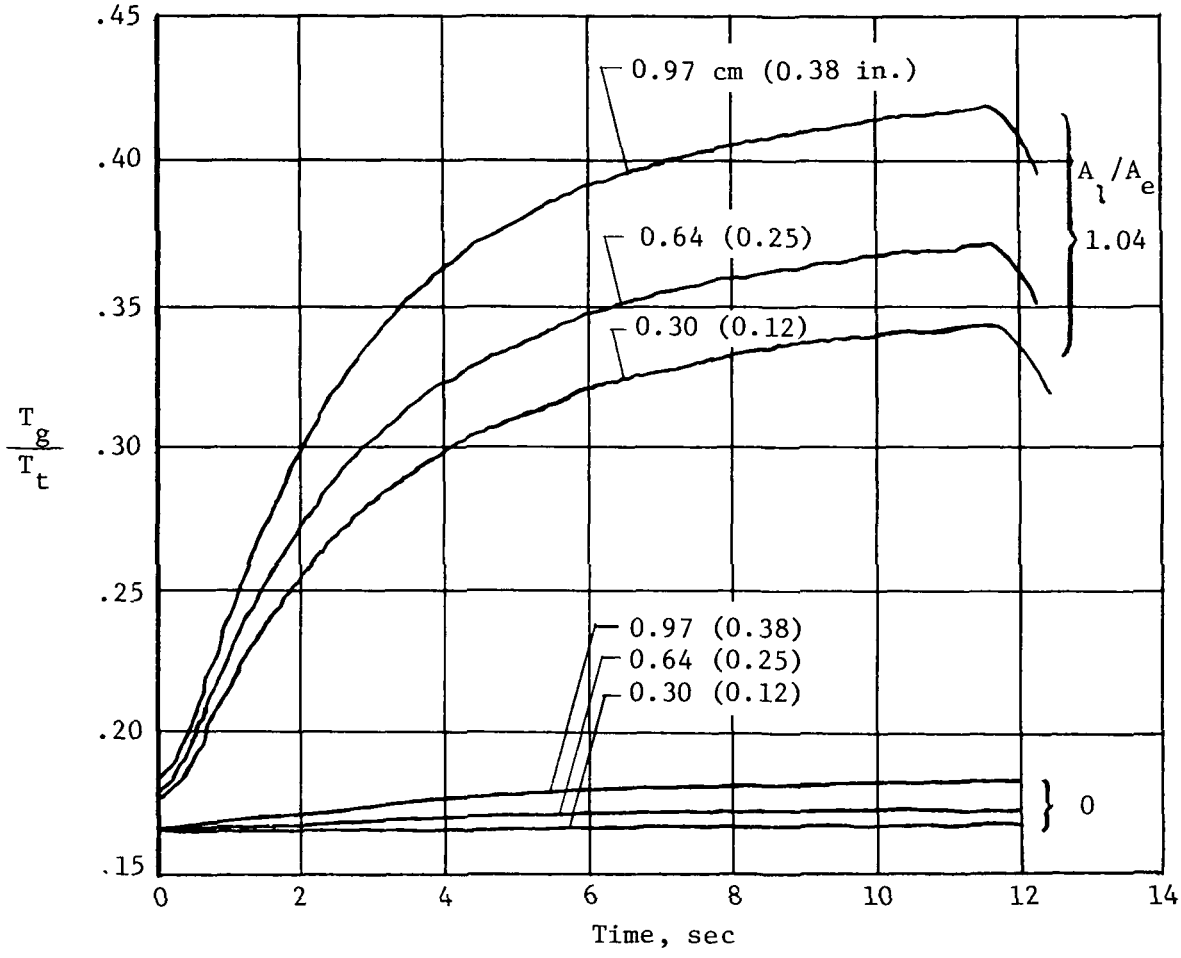

(c) Effect of distance from wall, near cove seal (location b, fig. 6).

Figure 14.- Concluded.

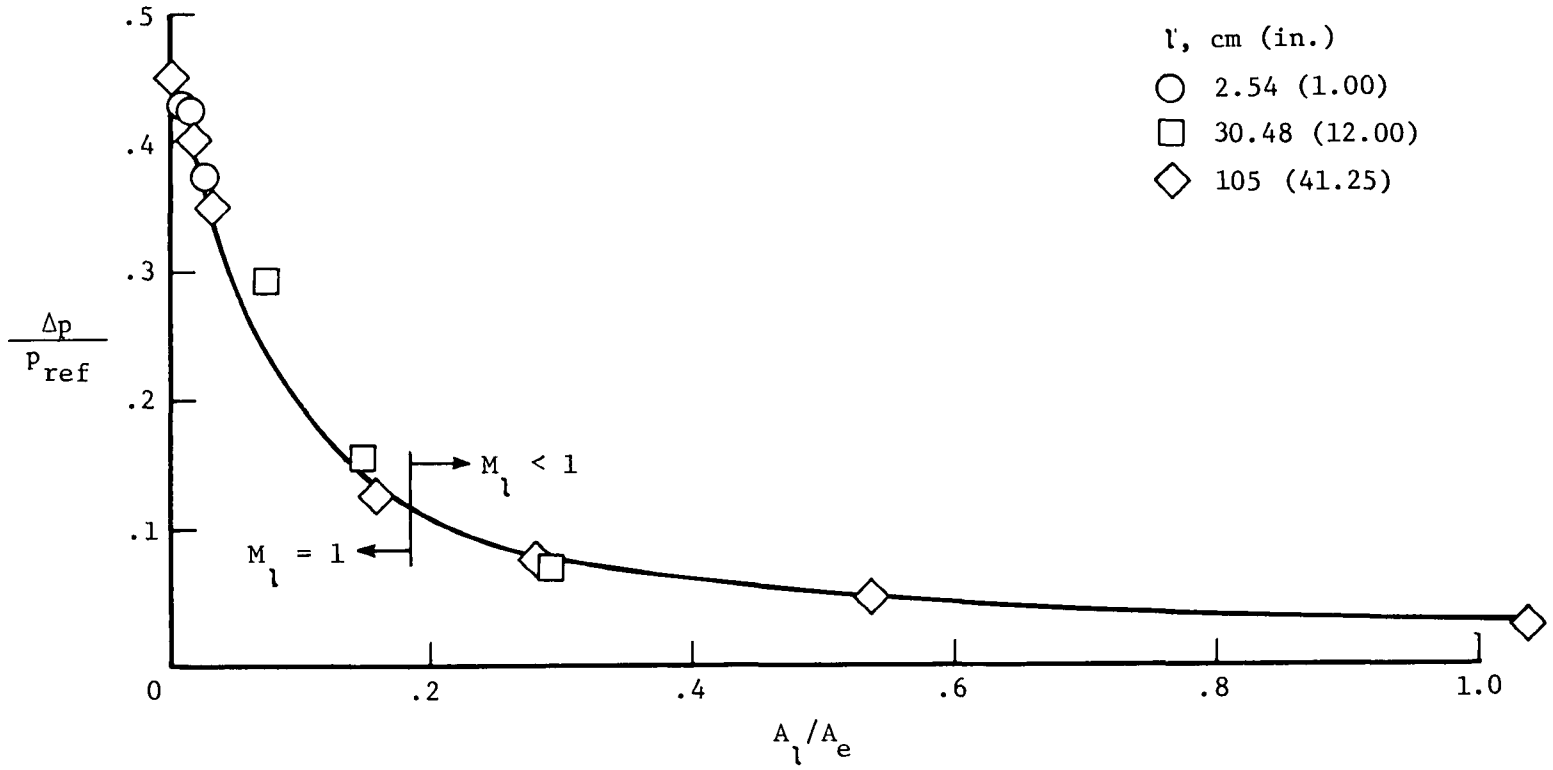

Figure 15.- Differential pressure loading across seal as a function of leak area. Attached flow; $R_\infty = 4.40 \times 10^6$ per meter (1.34×10^6 per foot); $T_t = 1888$ K (3400° R); $\alpha = 12°$; $\delta = 10°$.

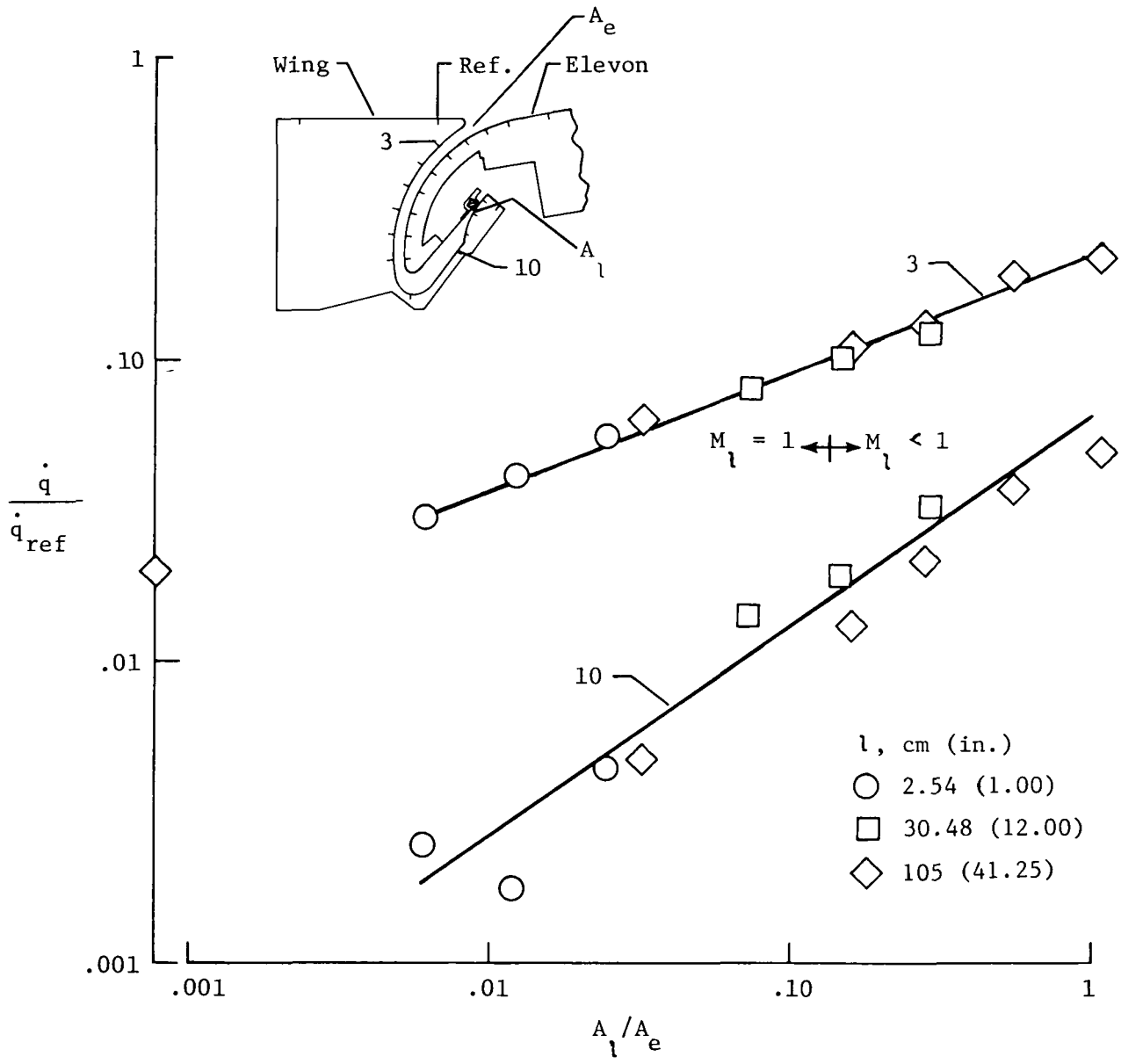

Figure 16.- Cove heating as a function of leak area. Attached flow; $R_\infty = 4.40 \times 10^6$ per meter (1.34×10^6 per foot); $T_t = 1888$ K (3400° R); $\alpha = 12°$; $\delta = 10°$.

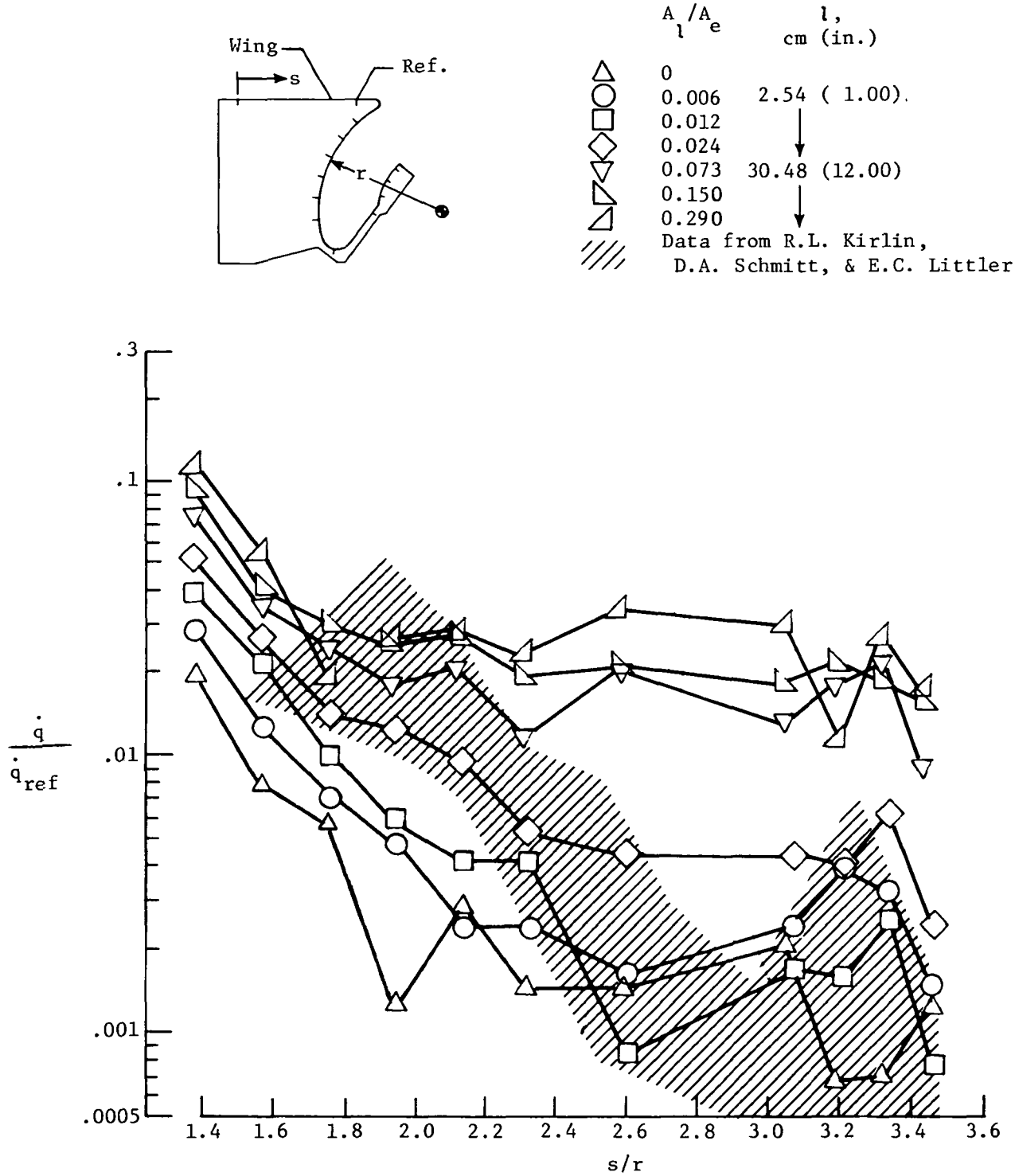

Figure 17.- Cove cold-wall heating-rate distributions for slotted leaks. Attached flow; $R_\infty = 4.40 \times 10^6$ per meter (1.34×10^6 per foot); $T_t = 1888$ K (3400° R); $\alpha = 12^\circ$; $\delta = 10^\circ$.

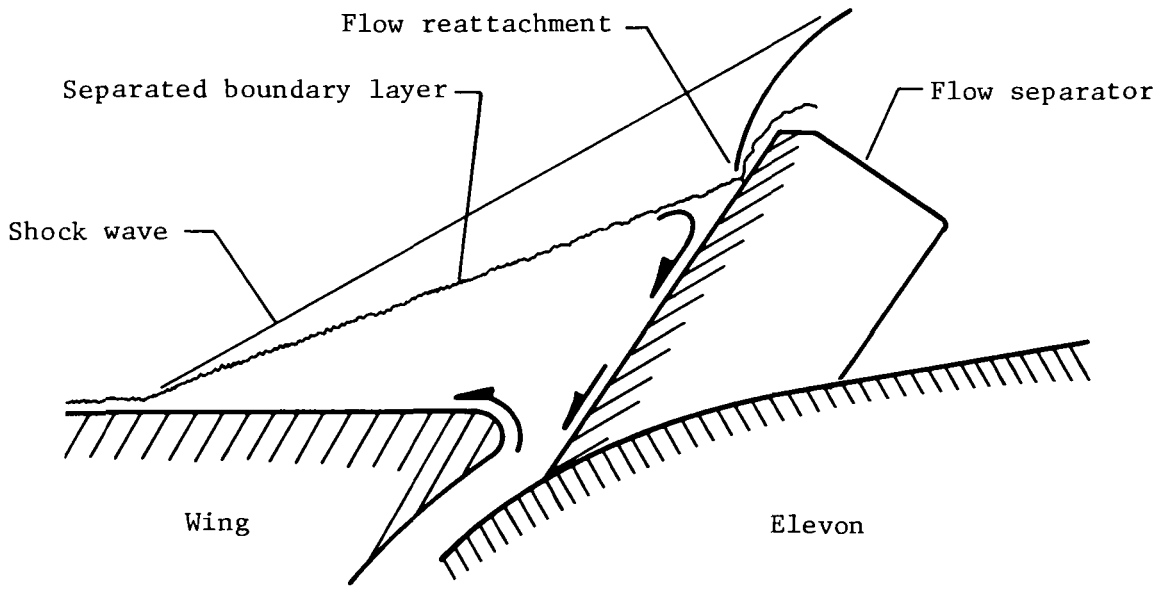

Figure 18.- Simplified flow details across cove entrance for separated flow.

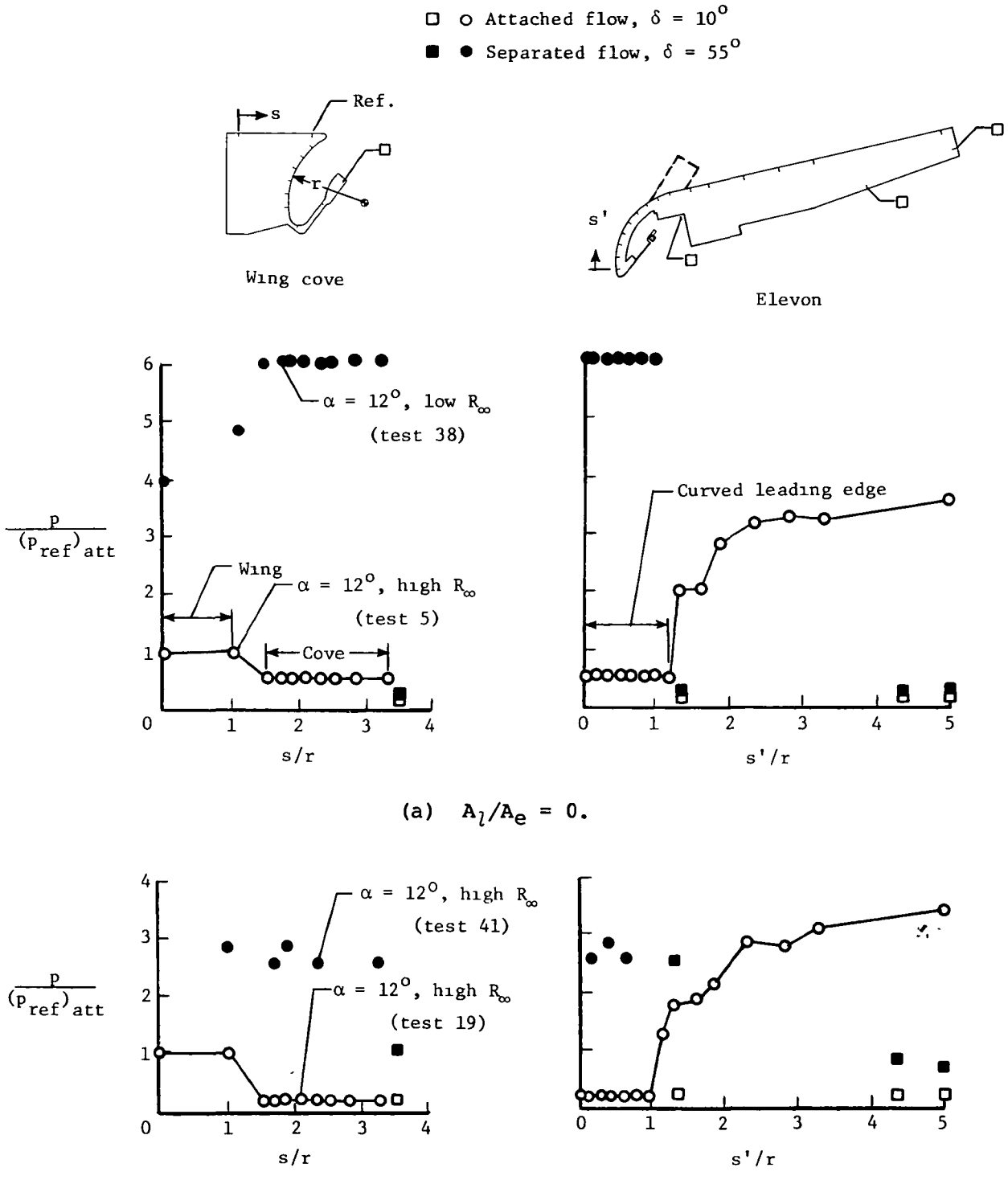

Figure 19.- Comparison of cove centerline pressure distributions for attached and separated flows. T_t = 1888 K (3400° R).

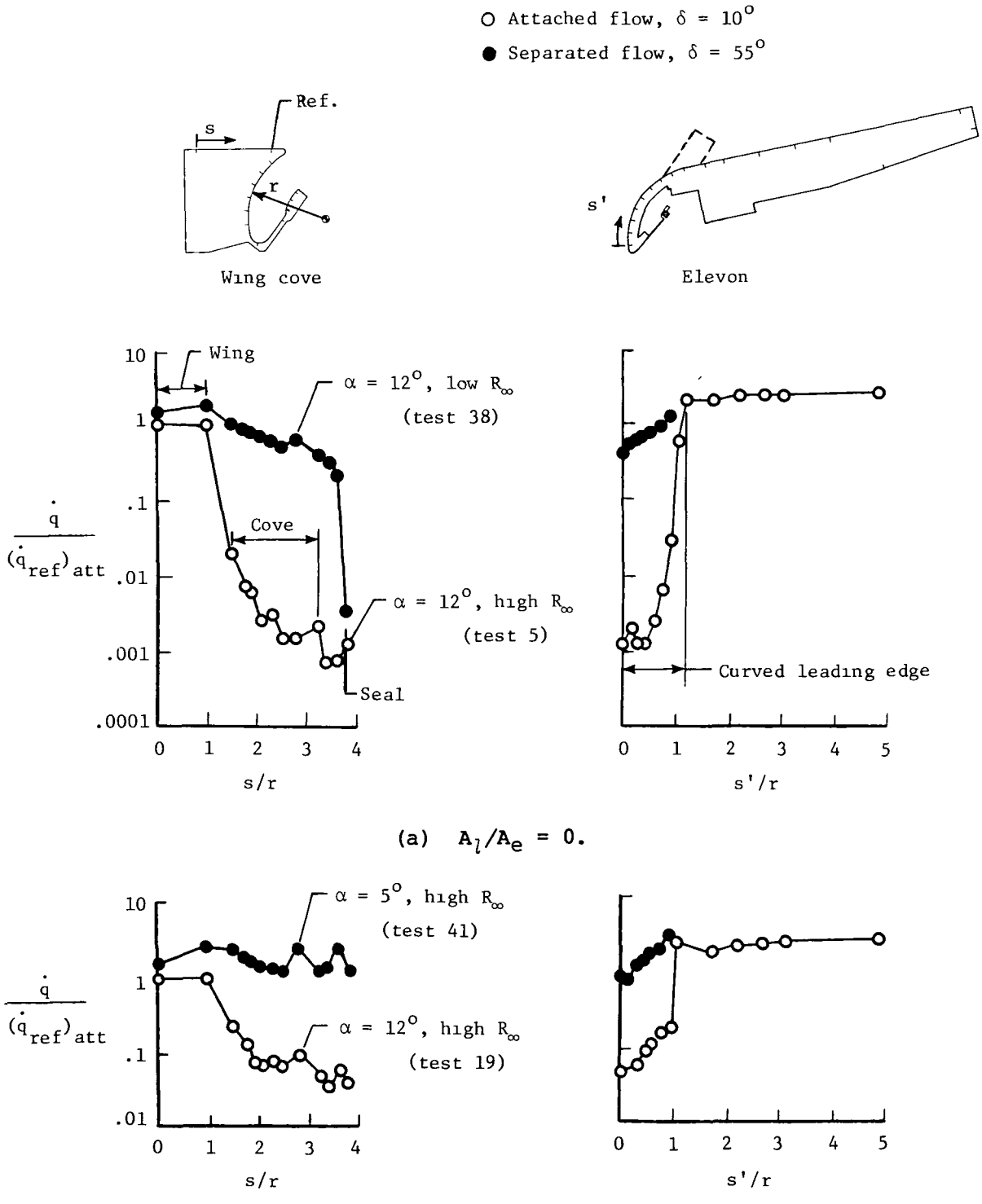

Figure 20.- Comparison of cove centerline cold-wall heating-rate distributions for attached and separated flows. T_t = 1888 K (3400° R).

1 Report No	2 Government Accession No	3 Recipient's Catalog No
NASA TM-74095		

4 Title and Subtitle	5 Report Date
PRESSURE AND HEAT-TRANSFER DISTRIBUTIONS IN A SIMULATED WING-ELEVON COVE WITH VARIABLE LEAKAGE AT A FREE-STREAM MACH NUMBER OF 6.9	December 1978
	6 Performing Organization Code
7 Author(s)	8 Performing Organization Report No
William D. Deveikis and Whitney Bartlett	L-12591
	10 Work Unit No
9 Performing Organization Name and Address	506-17-22-01
NASA Langley Research Center Hampton, VA 23665	11 Contract or Grant No
	13 Type of Report and Period Covered
12 Sponsoring Agency Name and Address	Technical Memorandum
National Aeronautics and Space Administration Washington, DC 20546	14 Sponsoring Agency Code

15 Supplementary Notes

16 Abstract

An experimental aerodynamic heating investigation was conducted to determine effects of hot boundary-layer ingestion into the cove on the windward surface between a wing and elevon for cove seal leak areas nominally between 0 and 100 percent of cove entrance area. Pressure and heating-rate distributions were obtained on the wing and elevon surfaces and on the cove walls of a full-scale model that represented a section of the cove region on the space shuttle orbiter. Data were obtained for both attached and separated turbulent boundary layers upstream of the unswept cove entrance. Average free-stream Mach number was 6.9, average free-stream unit Reynolds numbers were 1.31×10^6 and 4.40×10^6 per meter (0.40×10^6 and 1.34×10^6 per foot), and average total temperature was 1888 K (3400° R). Cove pressures and heating rates varied as a function of seal leak area independent of leak aspect ratio. Although cove heating rates for attached flow did not appear intolerable, it was postulated that convective heating in the cove may increase with time. For separated flow, the cove environment was considered too severe for unprotected interior structures of control surfaces.

17 Key Words (Suggested by Author(s))	18 Distribution Statement
Control-surface cove leakage Attached and separated flow Heat transfer Pressure Turbulent	Unclassified - Unlimited Subject Category 34

19 Security Classif (of this report)	20 Security Classif (of this page)	21 No of Pages	22 Price*
Unclassified	Unclassified	50	$4.50

* For sale by the National Technical Information Service, Springfield, Virginia 22161

NASA-Langley, 1979

National Aeronautics and
Space Administration

Washington, D.C.
20546

Official Business
Penalty for Private Use, $300

THIRD-CLASS BULK RATE

Postage and Fees Paid
National Aeronautics and
Space Administration
NASA-451

U.S.MAIL

10 2 1U,D, 010879 S90844HU
MCDONNELL DOUGLAS CORP
ATTN: PUBLICATIONS GROUP PR 15246-A
P O BOX 516
ST LOUIS MO 63166

NASA

POSTMASTER. If Undeliverable (Section 158 Postal Manual) Do Not Return

R J Krieger E241/Bldg/25987